JOURNAL OF GEOPHYSICAL RESEARCH, VOL. 104, NO. B12, PAGES 29,095-29,112, DECEMBER 10, 1999

Life cycle of the East Carpathian orogen: Erosion history of a doubly vergent critical wedge assessed by fission track thermochronology

Carlo A. E. Sanders,[1] P. A. M. Andriessen, and S. A. P. L. Cloetingh

Institute of Earth Sciences, Vrije Universiteit, Amsterdam, Netherlands

Abstract. Apatite fission track (FT) thermochronology applied to the East Carpathian fold-and-thrust belt in Romania constrains the interaction between the erosion history and the tectonic evolution of the orogen. The long-lived constant asymmetric topography of the orogen and the erosion pattern as inferred from apatite FT data are in agreement with the style of evolution predicted by doubly vergent critical Coulomb wedge models. During the Miocene, up to 4 km of erosion took place over the actively deforming orogen, and the erosion patterns forms a mirrored image of the subsurface deforming wedge. The erosion products are deposited in flanking molasse basins which subsided contemporaneously due to the growing topographic weight of the wedge. Deformation of the wedge was presumably active from the early to late Miocene, but apatite FT ages between 14 and 9 Ma and track length modeling predict an acceleration of erosion rates (0.5-0.3 mm/yr) initially in the middle to late Miocene (≈13±2 Ma). The onset of erosion coincides with the last phase of convergence and a climax in the deformation history. These features are interpreted to have been caused by underplating of the European continental margin. Convergence ceased before the Pliocene according to the activity of thrust faults. During the Pliocene and Quaternary, up to 2 km of overburden was removed by erosion, leading to isostatic rock uplift of the entire region. The use of apatite fission track "minimum ages" supports the general idea that the orogen has a diachronous evolution from north to south. The orogen in the southern Bend Zone has a more juvenile tectonic character, and the main erosion phase took place during the Pliocene and Quaternary (≈5-0 Ma). The integrated approach of large scale morphology and fission track analysis confirms the applicability of the theoretical Coulomb wedge mechanics to a natural compressive fold-and-thrust belt. The study complements the geometric features of the orogenic wedge with quantified erosion histories and illustrates the effects of orogen evolution on vertical movements in the entire convergent setting.

1. Introduction

Frontal parts of oceanic accretionary wedges and fold-and-thrust belts are well understood through the mechanics of critical Mohr-Coulomb wedges [*Chapple*, 1978; *Davis et al.*, 1983; *Dahlen et al.*, 1984]. The fundamental principles are illustrated in Figure 1a [e.g., *Davis et al., 1983*] in a simplified model based on analogue sandbox experiments: Sediments in front of a rigid backstop of infinite height are scraped from a continuously subducting plate and stacked in a wedge. The wedge attains a minimum critical taper ($\alpha+\beta$) and grows in a self similar way [*Dahlen*, 1990] by a process of alternating frontal accretion and internal deformation. The ratio of internal friction coefficient (μ_i) in the wedge and friction coefficient along the decollement (μ_b) are the main factors controlling the angle of the critical taper. The wedge-forming mechanism is independent of scale, and the "bulldozer" concept showed satisfying geometric resemblances with natural examples like Taiwan [e.g., *Dahlen et al.*, 1984]. These studies provided valuable insights on the mechanism of deformation, but the infinite height of the experimental backstop was an unrealistic assumption for natural orogens.

The use of backstops with finite height resulted in significantly different wedge geometries [e.g., *Malavieille*, 1984; *Byrne et al.*, 1993; *Willet et al.*, 1993; *Koons*, 1989, 1990], although the deformation mechanism remained the same (Figure 1b). The frontal part (or prowedge) still behaves as in the minimum tapered bulldozer model (Figure 1a), but differences occur to the rear above the tip of the backstop. The tip of the backstop is a velocity discontinuum which in numerical simulations is termed a singularity point [*Willet et al.*, 1993]. Above the singularity point forms an outer-arc-high, and in the same zone the stress regime flips orientation. To the rear, an oppositely tapering inner deformation belt (or retrowedge) is formed, characterized by a reversal in thrust vergence with respect to the prowedge (Figure 1b). This retrowedge approaches a maximum critical taper because material is essentially added to its back [*Wang & Davis*, 1996]. As a consequence, the prowedge and retrowedge have different height-width ratios, creating the generally recognized asymmetric geometry of the combined doubly vergent wedge.

Byrne et al. [1993] have shown that the key features described above are insensitive to the geometry of a backstop as long as it is situated at depth. The doubly vergent wedge has been recognized only in modern active orogens [*Koons*, 1995; *Beaumont et al.*, 1996; *Torrini and Speed*, 1989; *Silver and Reed*, 1988].

[1]Now at Midland Valley Exploration Limited, Glasgow, Scotland, United Kingdom.

Paper number 1998JB900046.
0148-0227/99/1998JB900046$09.00

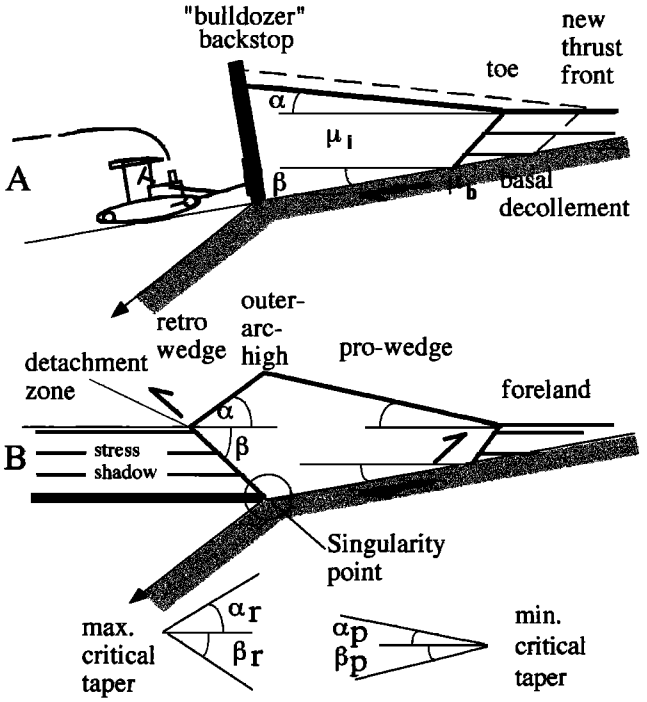

Figure 1. Diagram explaining mechanism of critical Coulomb wedges. (a) Bulldozer model: Sediments in front of a backstop (black) are scraped from a subducting plate (gray). The wedge grows in a self-similar way (stippled) according to a minimum critical taper ($\alpha+\beta$). Here μ_i is internal friction coefficient; μ_b is friction along basal decollement. (b) Doubly vergent critical wedge. See text for explanation. Horizontal hatching is undeformed sediments; arrows illustrate opposite thrust vergence; α_p and α_r are surface slopes of prowedge and retrowedge, respectively; β_r is angle between horizontal and detachment zone (retrowedge), and β_p is angle between horizontal and basal decollement of the prowedge.

The fundamental concept of the doubly vergent wedge is theoretically well analyzed, but still needs testing and validation against the complexity of natural examples. We tested the doubly vergent critical wedge concept against observations in the East Carpathian fold-and-thrust belt in Romania using the large-scale geomorphology and structural field studies. An extra tool we present is the erosion pattern of the mountain belt as reconstructed with the use of apatite thermochronology data, which can potentially distinguish between proposed geophysical models. *Kamp et al.* [1989], for example, have shown that cooling histories of rocks form information critical to constraining the underlying deformation mechanics for the Southern Alps in New Zealand. The Southern Alps are a well-known natural example of a doubly vergent orogenic wedge [*Koons,* 1994; *Beaumont et al.,* 1996]. However, the Southern Alps are a compressional oblique-slip orogen where deformation in the deeper crust is no longer controlled by friction but by time-dependent viscous behavior which influences the morphology of the orogen [*Beaumont et al.,* 1996]. Moreover, amounts of uplift and erosion rates have high values (18 km and 2.5 mm/yr, respectively) [*Kamp and Tippett,* 1993; *Tippet and Kamp,* 1993], which greatly influences the thermal structure of the orogen [*Koons,* 1987; *Stüwe et al.,* 1994] and complicates interpretation of cooling data [*Brown and Summerfield,* 1997].

The East Carpathians, on the other hand, form a closer natural analogue of a critical Coulomb wedge. It is a classical thin-skinned fold-and-thrust belt, with a relatively shallow basal decollement (maximum of 10 km deep) and is therefore supposed to deform entirely according to the (frictional) Mohr-Coulomb criterion. Substantial strike-slip displacements have never been identified in this part of the orogen. Moreover, the effects of the orogen formation on the subsidence and sedimentation history of its adjacent basins can be taken into account because they are presently exposed and well studied. With this new approach the tectonic history of the East Carpathians can be interpreted in the context of the critical wedge theory, in contrast to the descriptive concepts published so far. We concentrate on the Neogene tectonic history of the Romanian East Carpathians and use the doubly vergent critical wedge concept as a working hypothesis.

2. Regional Geological Setting

The Carpathian orogen is part of the European Alpine chain. It was formed by convergence of allochtonous microcontinents (intra-Carpathian plate) with the European foreland during the Cretaceous and Neogene. The Paleogene was a period of tectonic quiescence. During the Neogene the microcontinents collided en bloc with the European continental margin [*Burchfiel,* 1980; *Sandulescu,* 1988; *Csontos,* 1995]. In Romania the collision formed an orocline comprising the East Carpathians and Southern Carpathians, which at present reach maximum elevations of approximately 2000 m above sea level.

In the East Carpathians, three structural units are distinguished according to their tectogenetic history (Figure 2). From young to old (mainly after *Sandulescu et al.* [1981a, b]) they are the Moldavides (Neogene thrust belt), the Outer Dacides (Cretaceous thrust belt), and the Middle Dacides (allochtonous crystalline basement).

The Moldavides occupy the main part of the orogen and are situated on its most eastern side. The nappe systems are made up of flysch sediments with stratigraphic ages ranging from late Early Cretaceous in the internal nappes to middle Miocene in the more external nappes. The most external and youngest nappe consists mostly of molasse sediments. According to *Sandulescu* [1988], the nappes were progressively emplaced on the European foreland from 22 to 10 Ma (early to late Miocene).

The Outer Dacides lie to the west of the Moldavides. Stratigraphic ages of the flysch sediments range from Early to Late Cretaceous [*Sandulescu et al.,* 1981a]. The main phase of thrusting in the Outer Dacides took place during the Late Cretaceous. The third and most internal unit is formed by the Middle Dacides, consisting of crystalline basement rocks with Mesozoic and Cenozoic sedimentary cover. The nappe structure was formed in the early Late Cretaceous.

The observed present-day configuration was basically achieved by a three-step evolution (Figure 3). Closure of the Outer Dacidian flysch trough during the late Early to Late Cretaceous (130-66 Ma) by subduction of oceanic(?) crust under the allochtonous microcontinent (Middle Dacides) resulting in the formation of an (old) accretionary wedge (Outer Dacides). A period of tectonic quiescence followed during the Paleogene (Figure 3b) with extensive flysch sedimentation from foreland and hinterland sources to the Moldavide trough. Renewed convergence during the Neogene by westward subduc-

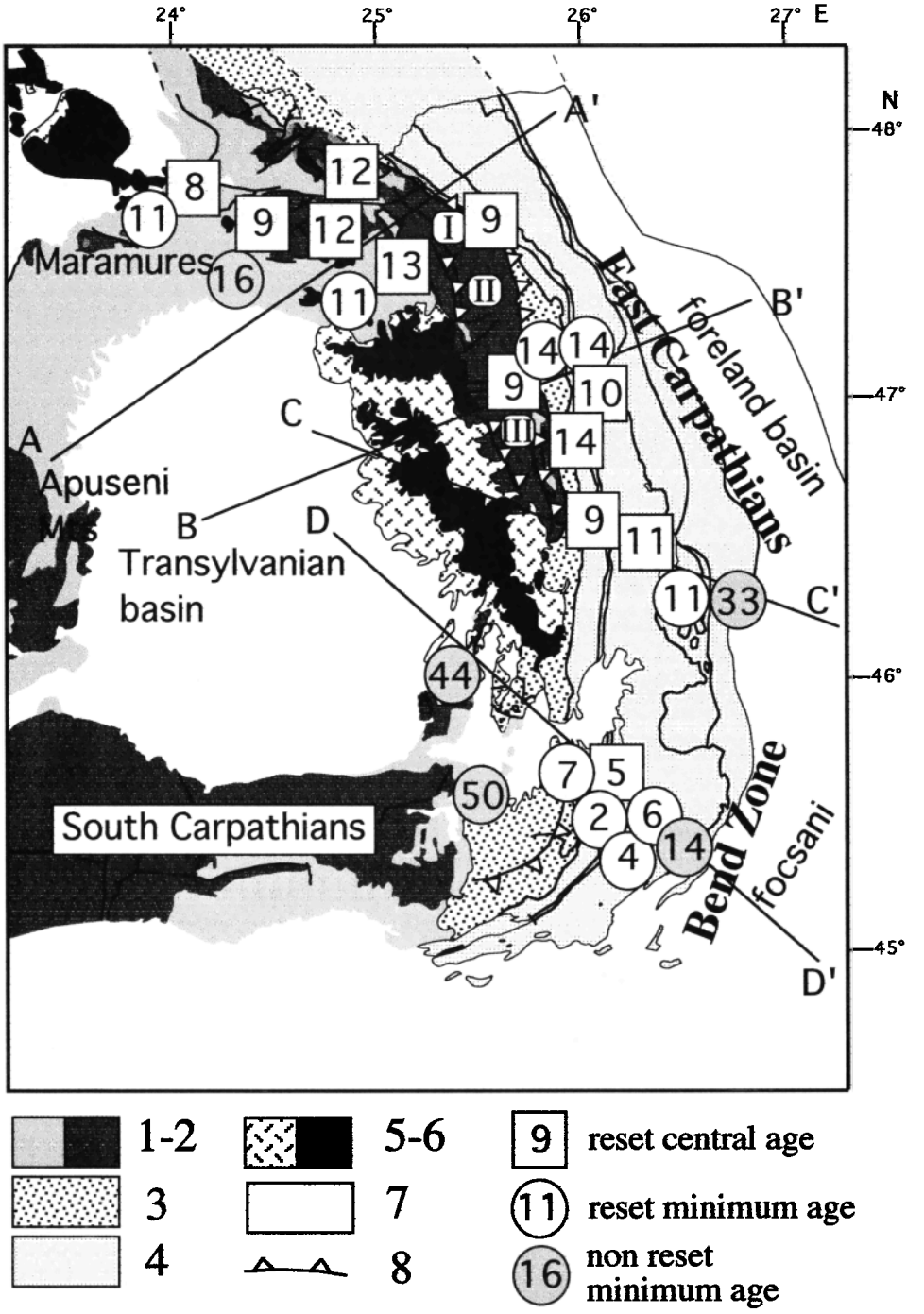

Figure 2. Tectogenetic map of Romania after *Sandulescu et al.* [1978]. Legend: 1 and 2, allochthonous plate: 1, sedimentary cover (Senonian-Neogene); 2, Middle Dacides (crystalline basement); 3, Outer Dacides (flysch); 4, Moldavides (flysch); 5, Neogene volcanics (extrusive); 6, intrusive; 7, Miocene-Quaternary molasse; 8, retrovergent thrusts (see discussion). Roman numbers are localities referred to in text; A-A' to D-D' are profiles from Figures 4 and 5.

tion and underplating of the European continental margin led to the closure of the Moldavide flysch trough and formation of a fold-and-thrust belt (Figure 3c). Balancing cross sections by restoration of thrust sheets [*Roure et al.*, 1993; *Ellouz and Roca*, 1994; *Morley*, 1996] showed that a minimum shortening of 130-220 km occurred during the Neogene, indicating a subduction rate in the order of 10-15 km/Ma.

During the final phase of convergence, molasse basins formed on both sides of the orogen. A late Neogene calc-alkaline volcanic arc formed in the allochtonous plate, intruding both the molasse basin and the flanking areas of the orogen (Figure 2 and 3). Convergence finally stopped with collision (docking) of the allochtonous plate against the European foreland during the late Miocene.

Tectonic activity is presumably diachronous from north to south along the orogen, as indicated by both the last activity of the thrust front [*Sandulescu et al.*, 1981a, b] and the eruption ages of the volcanic chain [*Pecskay et al.*, 1995]. The

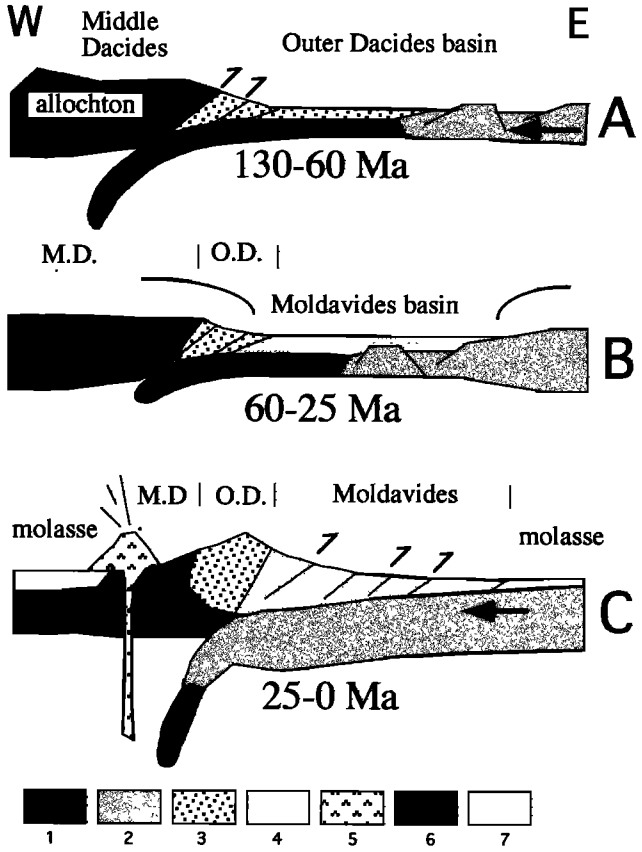

Figure 3. Diagram sketching the tectonic history of the East Carpathians. European foreland is to the east. (a) Cretaceous convergence by subduction of oceanic lithosphere: formation of Middle and Outer Dacides (MD and OD), (b) Paleogene flysch sedimentation in Moldavide trough in front of a passive margin, and (c) renewed convergence in Neogene forming East Carpathian orogen, resulting in thrusting of Moldavides and underplating of European continental margin. Legend: 1, allochthonous continental crust; 2, European continental crust; 3, Outer Dacides flysch; 4, Moldavides flysch; 5, Neogene volcanic chain; 6, oceanic crust; 7, molasse.

ages of both processes show a trend from late Miocene in the north to Pliocene-Quaternary in the Bend Zone. Therefore the northern and central East Carpathians ("East Carpathians sensu stricto") are treated as one unit separately from the southern sector ("Bend Zone") throughout this paper.

3. Approach to Investigation

We first identify the surface expression of the doubly vergent wedge by its present day topography. Subsequently we make an inventory of the information that is available on the known subsurface geometry and active structures. With the integrated information an attempt is made to constrain the outline of the deforming orogenic wedge in the East Carpathians. We next determine the erosion history of the area with the apatite fission track thermochronology method and evaluate if the erosion history is in accordance with theoretical predictions. Finally, we revisit and evaluate our working hypothesis and compare with other models after we have shown the validity of the concept for the East Carpathian orogen. We subsequently integrate the observations on erosion, deformation, and sedimentation in the critical wedge concept to discuss the evolution of the East Carpathian orogen.

Note that in this paper we use the terms rock uplift, surface uplift, and exhumation as did *England and Molnar* [1990]; that is rock and surface uplift are with respect to a reference frame (geoid or mean sea level), and exhumation is rock uplift with respect to the local mean surface elevation [see also *Brown*, 1991]. When no information of the local Earth surface is available, the general term "erosion" is used for all removal of overburden.

4. Orogen Morphology and the Subsurface Wedge

All critical doubly vergent Coulomb wedges have a number of fundamental geometric features in common that form the main criteria to recognize a doubly vergent wedge in nature (Figure 1b) [*Koons*, 1990; *Byrne et al.*, 1993]: 1) Doubly vergent wedges are asymmetric with short and steep retrowedges opposing long and gentle inclined prowedges. 2) The dominant thrusts have opposite vergence in the two wedges. 3) The "outer arc high" represents the highest peaks and coincides with the main drainage divide; it forms the transition zone between the two opposing wedges which is situated roughly on top of the singularity point. 4) The retroforeland above the backstop is protected against deformation by a stress shadow. Also, the peripheral foreland basin in front of the prowedge is not deformed since no differential movement takes place along the basal decollement here. By analyzing the structures and the large-scale geomorphology of the East Carpathian orogen we want to see if these features are retained in an ancient orogen.

Four topographic profiles in the East Carpathians show a similar asymmetry (Figure 4). The eastern part of the profile is formed by a gently inclined mean surface slope of α_p = 0.8° to 1.4° (regression fit over topographic summits), representing the surface slope of the prowedge. The main drainage divide (outer-arc-high) reaches peaks of up to 1900 m above sea level. The western flank of the orogen is formed by a relatively steep surface slope (α_r = 2.8° to 4.8°) with a sharp boundary (topographic kink) to the retroforeland. This is the surface slope of the retrowedge. The ratio between the length of the prowedge and the length of the retrowedge is approximately 3:1 (except for profile B-B'), which is close to observations from other natural doubly vergent wedges [*Silver and Reed*, 1988]. The retroforeland (Transylvanian Basin) and the proforeland are essentially undeformed [*Ciupagea et al.*, 1970; *Huismans et al.*, 1997] and have a semihorizontal surface slope.

The subsurface outline of the prowedge is available from published geological sections [*Stefanescu*, 1985], where the basal decollement is a clear reflector on seismic profiles [*Mocanu et al.*, 1996]. Overall, decollement angles (β_p; see Figure 5) vary between 4° and 6.5°. The total taper of the prowedge ($\alpha_p+\beta_p$) is fairly constant in the East Carpathians and varies between 4.8° and 7.4°, which coincides well with critical tapers of other natural settings [*Davis et al.*, 1983; *Dahlen*, 1990].

The detachment zone is a lineament from the singularity point to the toe of the retroslope which separates deforming material in the retrowedge from essentially undeformed material below. From models and natural examples (e.g., Southern Alps, New Zealand) we know that the lineament is expressed as a localization of strain which we will call here the "detachment zone." A detachment zone has never been identified as such in the East Carpathians, probably because its existence was not

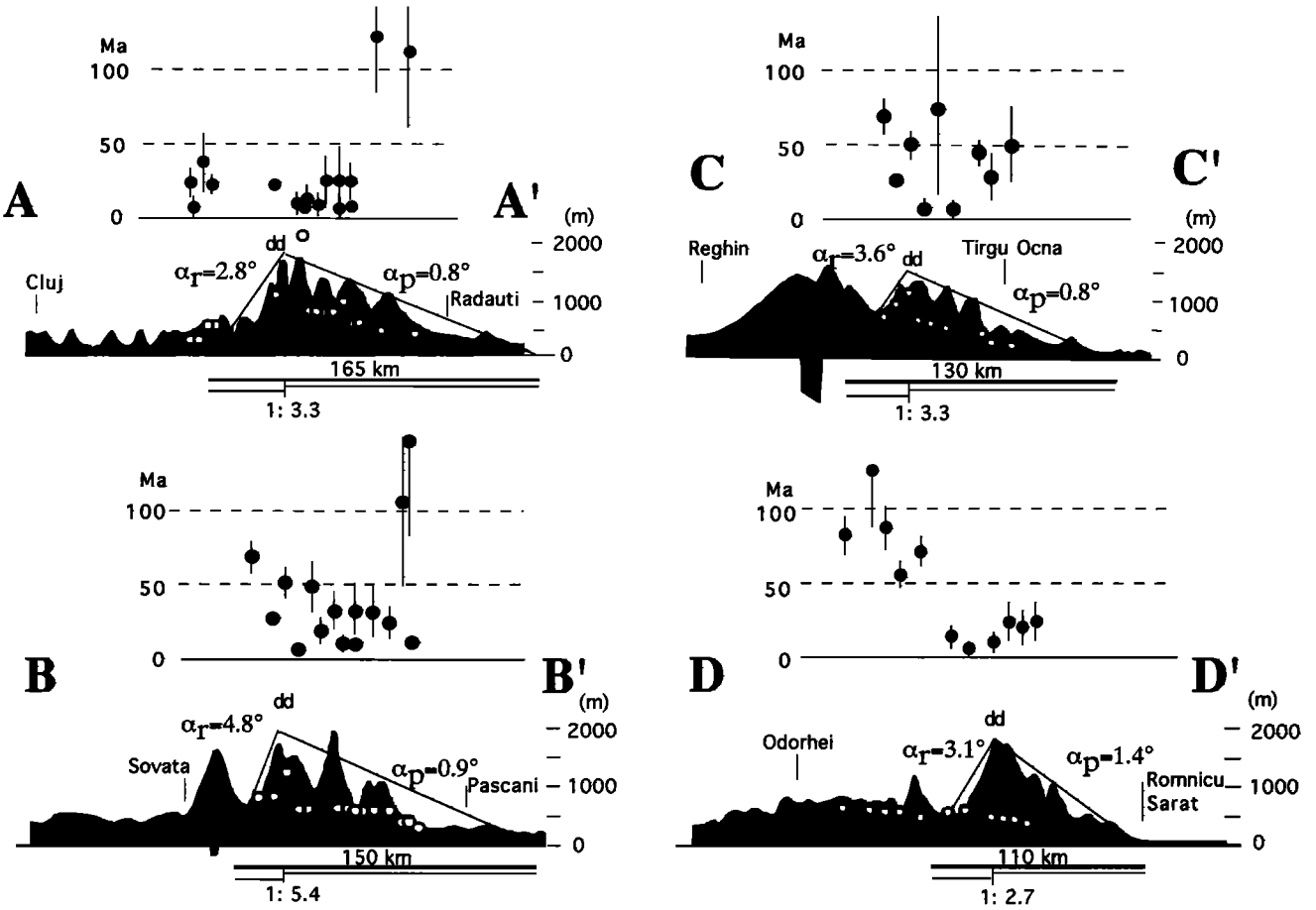

Figure 4. Morphological profiles and fission track age pattern (33x vertical exaggerated): outline of best fit surface slope (α_p and α_r) over peaks; volcanics are black; open circles are fission track (FT) sample locations projected on profile line with respect to main drainage divide (dd). Plotted directly above the sample locations are the corresponding FT central ages (solid circles) with two sigma error bars.

anticipated (see below). We inferred the position of the singularity point at the contact between the subducting frontal decollement (foreland plate) and the tip of the crystalline allochtonous plate on the basis of sections by *Stefanescu* [1985]. It coincides with the deepest point of the sedimentary wedge (approximately 10 km under the outer-arc-high). Constructed detachment zone dips (β_r) vary between 13° and 19° for the sections in the East Carpathians (Figure 5). The total taper of the retrowedge ($\alpha_r+\beta_r$) (although less well constrained then the prowedge) varies between 15° and 22°.

5. Structural Control

An essential aspect of the doubly vergent wedges is that the prowedge and retrowedge have opposite vergent dominant thrust systems [e.g., *Malavieille*, 1984; *Koons*, 1990]. The prowedge of the East Carpathians has predominantly east vergent thrusts. In the retrowedge the vergence of Miocene thrusts is difficult to identify because of relict (both east and west vergent) faults caused by older (Cretaceous) deformation phases. Because of the relatively old age of the rocks (Palaeozoic to Cretaceous) it is difficult to date Miocene activity of the structures in this area.

Published geological maps and sections [*Stefanescu*, 1985] of the East Carpathians, in general, show a remarkable increase in the areal density of retrovergent faults as the retrowedge is approached. Those occurring in the Middle Dacides crystalline basement have formerly been interpreted as folded faults originating from Cretaceous deformation phases. *Sandulescu et al.*, [1981b], however, already mentioned a possible reactivated component during the Miocene.

Field studies (near the villages of Pojorita (I), Iacobeni (II), and Voslabeni and Lazarea (III) (see Figure 2), maps [*Balintoni et al.*, 1982; *Bercia et al.*, 1975; *Krautner et al.*, 1975, 1978; *Muresan et al.*, 1986; *Sandulescu et al.*, 1975], and sections [*Stefanescu*, 1985] on the retrowedge of the East Carpathians reveal a number of important east dipping faults with clear east-side-up displacements (Figure 2) and thus represent a retrovergent thrust system, opposite to the thrust system in the prowedge. The brittle character of these faults (in I, II and III) indicates that they deformed under low-temperature conditions and together with overprinting relationships suggests that they were active in a late phase of the deformation history.

Despite these indications it is difficult to prove that a retrovergent thrust system was dominant in the retrowedge during the Miocene orogenesis. The structural approach alone is not sufficient to identify an active retrowedge and the criterion of opposite thrust vergence in the opposing wedges remains inconclusive for the East Carpathians. A main boundary thrust as in the Southern Alps in New Zealand [*Kamp et al.*, 1989]

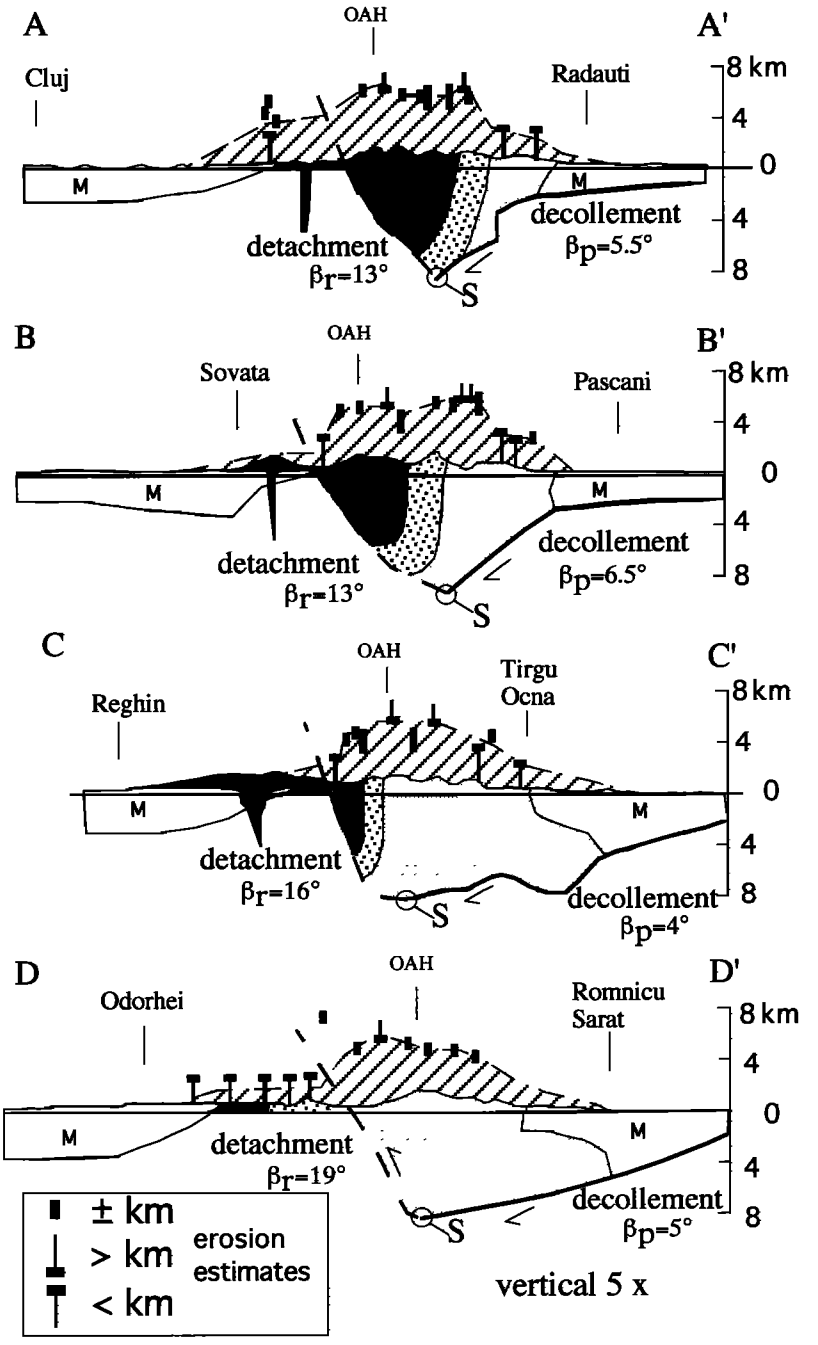

Figure 5. Geology and outline of subsurface wedge combined with erosion cumulatives: Profiles are the same as in Figure 4, but vertical exaggeration is less (5x). The basal decollement and internal geology are reconstructed from published sections (color schemes are as in Figure 2). β_p and β_r are overall angles of decollement and detachment surfaces with the horizontal. Arrows indicate relative movements. The cumulative amounts of erosion in kilometers (hatched) are based on estimates in Table 2. Cumulative sedimentation thickness of molasse (M) since the Badenian (17 Ma) is from literature.

has never been identified as such. Either it does not exist, which argues against the doubly vergent wedge concept, or it might be due to the lack of a significant strike-slip component in the Carpathians and/or the widespread posttectonic volcanic cover (Figure 2). In the Bend Zone a major retrovergent fault is present at the inferred location of the detachment zone (Figure 2).

Constraints on the timing of the structures in the prowedge are based on (overthrust-) stratigraphic arguments. Three distinct Miocene thrusting episodes have been recognized by *Sandulescu* [1988]. An early event during the early Miocene [20-18 Ma] records the onset of Neogene plate convergence. It is followed by a distinct early middle Miocene event (15 ma). The third and last phase of frontal thrust movement in the northern and central parts of the East Carpathians occurred in the Sarmatian (13-11 Ma) [*Sandulescu*, 1981b]. The last out-of-sequence deformation within the wedge is recorded in early Pannonian sediments (11-7 Ma) of the Comanesti Basin

[*Dumitrescu et al.*, 1970]. In the Bend Zone the last deformation is documented in the Pliocene-Quaternary, where large-scale folding and shortening of at least 22 km took place [*Ellouz et al.*, 1994; *Hyppolyte and Sandulescu*, 1996].

6. Erosion of Critical Wedges

The critical taper of an active Coulomb wedge is determined by the balance between vertical (lithostatic) and horizontal forces in every column of the wedge [*Dahlen*, 1990]. Ideally, any material eroded from a column decreases the vertical force, which triggers internal deformation in the wedge to restore the critical taper. The critical geometrical form of the wedge is thus unaffected by erosion, but its size is dependent on the mass outflux by erosion. It is argued by *Dahlen and Barr* [1989] that an active wedge eventually attains a steady state width when the influx of material at the toe is balanced by the outflux of material by erosion. A wedge in a destructive state, on the other hand, is reshaped by erosion processes [*Kooi and Beaumont*, 1996].

Erosion rates are strongly defined by the activity of weathering and transport processes at the Earth's surface, and these processes are mainly controlled by precipitation [*Beaumont et al.*, 1992; *Kooi and Beaumont*, 1996]. Therefore, the amount and distribution of precipitation over an active critical wedge is a major factor controlling where most erosion takes place. Because removal of overburden causes vertical advection and thus cooling of rocks, temperature histories as assessed with thermo-chronological techniques give important information about the erosion history [*Brown and Summerfield*, 1997; *England and Richardson*, 1977].

7. Apatite Fission Track Thermochronology

Thermal histories for the East Carpathians are reconstructed using the apatite fission track thermochronology (AFTT). AFTT is a well-established low-temperature thermochronology method [e.g. *Wagner and Van den Haute*, 1992; *Andriessen*, 1995] with a closure temperature [*Dodson*, 1973] of approximately 120°C over geological timescales (10^6-10^8 Ma). Fission tracks are not entirely stable and are healed by a process called annealing [*Green et al.*, 1986]. The nonlinear character of the annealing process has in practice led to a subdivision in the annealing ranges. Over geological timescales, annealing rates are very slow in apatite at temperatures below 60°C, and insignificant reduction in fission track lenths is observed. Mean fission track lengths in apatite are typically 14.5±0.5 μm [*Gleadow et al.*, 1986]. Annealing rates accelerate in the range from 60°C to 120°C, defining the Partial Annealing Zone (PAZ), which is characterized by mean track lengths between 9 and 14 μm [e.g., *Gleadow and Fitzgerald*, 1987]. Above 120°C, no tracks are preserved, defining the Total Annealing Zone (TAZ). Track length reduction affects measured ages directly [*Green*, 1988], and therefore the geological significance of measured ages has to be evaluated against track length data.

The annealing behavior of fission tracks in apatites is partly dependent upon the chemical composition of the host mineral (especially the fluorine-chlorine ratio) [*Green et al.*, 1986]. There is good evidence that F apatites anneal more readily than Cl apatites [*Green et al.*, 1986]. Conservative estimates indicate that tracks in F apatites are totally annealed at 110°C while Cl-rich apatites preserve tracks up to 130°C at a timescale of 10 Ma [*Crowley et al.*, 1991; *Burtner et al.*, 1994]. The differential annealing behavior leads to a wide spread of individual grain ages, particularly when samples reside in the temperature range between 90°C and 120°C. The spread in ages is statistically defined as the amount of dispersion [*Galbraith and Laslett*, 1993]. High dispersion (>30%) is taken as evidence that the grain ages of a sample do not represent a uniform grain age population. Note that in sediments, high dispersion can also be caused by different FT provenance ages.

Chemical variations among apatite grains within a sample can be recognized by studying the effects of etching. Apatites are chemically etched with HNO_3 to make the tracks microscopically visible for routine FT age determination procedures [*Ravenhurst and Donelick*, 1992]. Cl apatites (and the more rare OH apatites) have higher etch rates and therefore display larger etch pits than F apatites under the same etch conditions [*Burtner et al.*, 1994]. Etch pit dimensions parallel to the crystallographic c axis have been estimated under the microscope (in bins of 0.5 μm) simultaneously with FT age determination (magnification 1000x). On the basis of etch pit dimensions we classified F apatites (≤1.5 μm) and F-Cl-OH apatites (≥2 μm; in Table 2 labeled "Cl") after the method described by *Burtner et al.* [1994]. As we shall see later, chemistry variations are crucial when interpreting thermochronological histories of samples which resided between 90°C and 130°C.

7.1. Results

Fission track analyses on apatite were carried out using standard procedures [e.g., *Rohrman*, 1995; *Andriessen*, 1995] and the external detector method [*Hurford and Green*, 1982, 1983]. Four topographic profiles were sampled perpendicular to the strike of the orogen (Figures 4 and 6). Most samples analyzed come from approximately the same elevation (600±200 m) and consist of clastic sediments. The sampling of vertical sections was precluded by the lack of outcrop. Apatite fission track ages of 51 samples are presented as central ages (Ma) with one sigma error (Ma) and degree of dispersion (%) [*Galbraith and Laslett*, 1993] in Table 1.

Apatite FT central ages range from 5 to 170 Ma. The youngest ages (14-5 Ma) prevail in a zone along strike over the outer-arc-high of the East Carpathians and in the Maramures region (Figure 6). These samples have FT central ages and single grain ages all much younger than their stratigraphic ages (Table 1). They have low dispersion, representing a homogeneous age population (Figure 7e and 7f), including the samples where we documented significant variation in the chemical composition using the etch pit dimensions (Table 2 and Fig 7f). These samples are referred to as totally reset samples. Mean track lengths are typically 13±1.5 μm.

The totally reset samples are alternated with and flanked on either side by zones with increasingly older FT ages (12-37 Ma), characterized by high grain age dispersion. FT central ages and most single grain ages are younger than the stratigraphic age. A minor amount of single grain ages is older than the stratigraphic age, indicating partial annealing (Figures 7c and 7d). For some samples the high dispersion is due to high Cl content of the apatite grains since the older single grain ages generally have etch pits >1.5 μm (Figure 7d).

On the most external slopes of the mountain range and on the rim of the Transylvanian Basin are samples with central ages and most single grain ages equal to or older than the stratigraphic age (37-155 Ma) (Figure 7b). These samples have not been thermally disturbed since their deposition and have high dispersion because of different provenance ages of

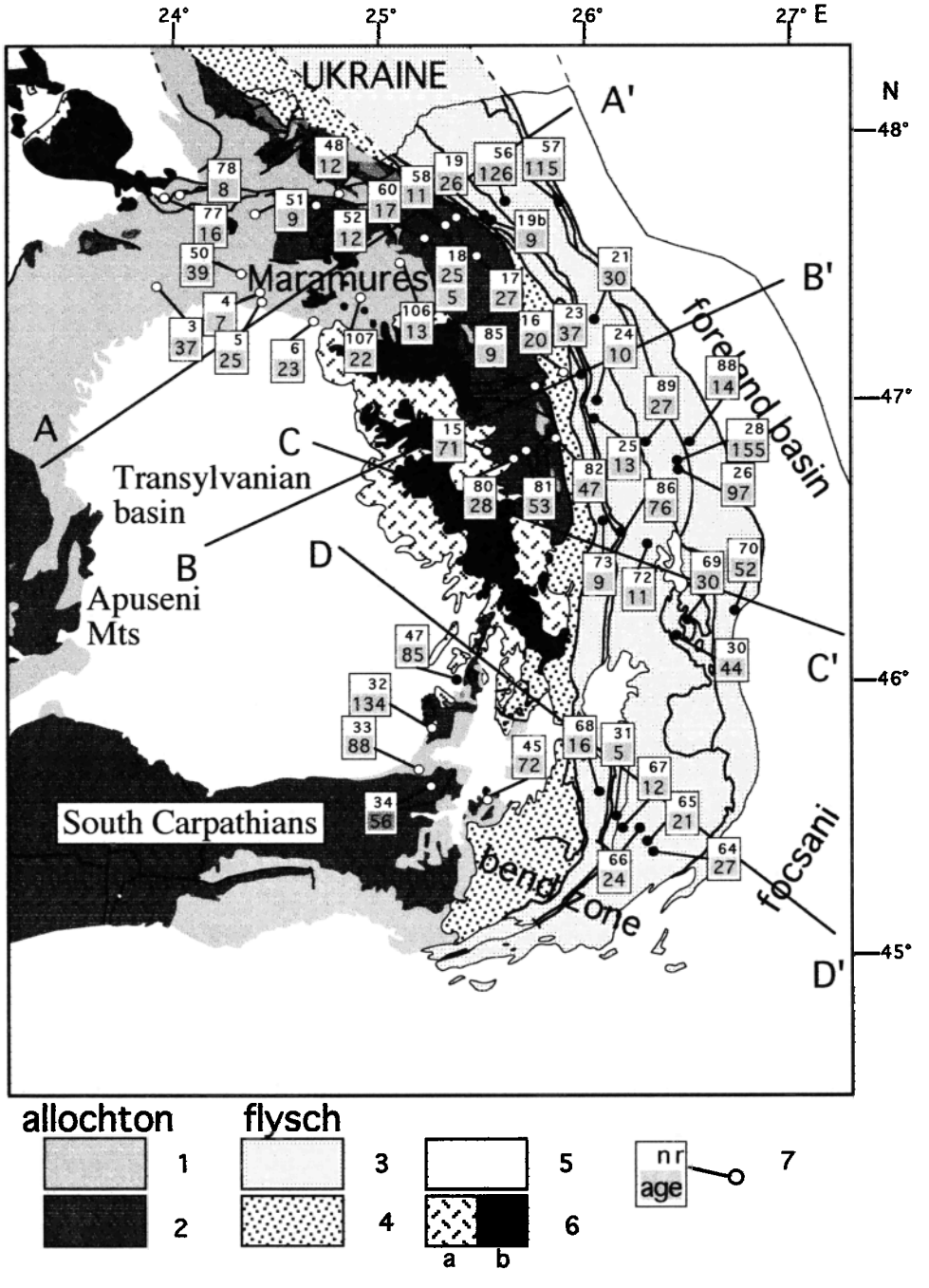

Figure 6. Tectogenetic map of Romania after *Sandulescu et al.* [1978] with FT central ages. A-A' to D-D' are profile lines of Figures 4 and 5. Legend: 1 and 2, allochthonous plate: 1, sedimentary cover (Senonian-Neogene); 2, Middle Dacides; 3, Moldavides; 4, Outer Dacides; 5, Miocene-Quaternary molasse; 6, Neogene (a) volcanic sediments and (b) intrusives; 7, FT sample locality, sample number, and central age.

the single grains. Two tuffaceous layers (samples 88-89) have FT central ages similar to their stratigraphic age (Table 1) and mean track length of 14±0.7 μm, reflecting a thermally undisturbed depositional age.

The crystalline basement has FT central ages ranging from 9 Ma near the outer-arc-high to 134 Ma next to the Transylvanian Basin, and dispersion is generally high. The mean length associated with the older FT ages varies between 11.2±1.6 and 13±1.5 μm and indicates slow cooling.

It is remarkable that no obvious relation of FT ages with the tectonic units can be recognized. When the FT ages are plotted as a function of topography (Figure 4), the profiles show a roughly similar trend linked to the morphology of the doubly vergent wedge. On the prowedge, FT central ages decrease gradually to the outer-arc-high, where they attain lowest values. The retrowedge has variable FT ages, but in the retroforeland, FT ages rapidly increase again. The trend in profile A-A' and B-B' is somewhat blurred because of the different pre-

Table 1. Fission Track Results

Lithology	Strat. Age	Sample	Elev., m	N Grains	Rho s (Ns) x 10^6/cm^2	Rho i (Ni) x10^6/cm^2	Rho d (Nd) x10^6/cm^2	C.A.±1σ, Ma	Disp., %	Mean L±1σ	N,L
Sandstone	Miocene	3*	500	20	0.3382 (224)	1.3060 (865)	0.0264 (3290)	37±4	14	13.0±1.4	21
Sandstone	Oligo-Miocene	4*	400	20	0.0506 (38)	1.5620 (1174)	0.0264 (3290)	7±2	81	10.2±2 3	6
Sandstone	Oligo-Miocene	5*	400	20	0.2042 (134)	1.5605 (1024)	0.0264 (3290)	25±5	73		
Dej tuff	Badenian	6*	600	20	0.1286 (80)	0.8020 (499)	0.0264 (3290)	23±3	8	12.1±0.9	13
Amphibolite	-	15	800	31	0.3877 (545)	0.8984 (1263)	0.0278 (2068)	71±6	16	13.0±1.5	100
Sandstone	Barr-Albian	16	600	39	0.1151 (117)	0.9169 (932)	0.0261 (1944)	19±4	75		
Schistone	-	17	800	22	0.0307 (19)	0.2184 (135)	0.0261 (1944)	27±9	69		
Quartzite	Cret.inf.	18(I)	1000	27	0.0075 (9)	0.2260 (272)	0.0277 (1975)	5±2	14		
Idem	idem	18(II)	1000	11	0.0350 (16)	0.3140 (124)	0.0261 (1944)	25±9	75		
Sandstone	Cret.	19	700	19	0.0796 (61)	1.3950 (535)	0.0261 (1944)	26±6	77		
Sandstone	Cret.	19b	700	42	0.0660 (145)	1.1368 (2497)	0.0261 (1944)	9±1	14	13.5±2.3	28
Sandstone	Oligocene	21	600	15	0.0914 (25)	0.6181 (169)	0.0261 (1944)	30±8	49		
Sandstone	Cret.inf.	23	600	48	0.0535 (63)	0.2556 (301)	0.0261 (1944)	36±6	49		
Sandstone	Eocene	24	600	34	0.0604 (53)	0.9204 (807)	0.0261 (1944)	10±2	14	13.9±0.8	10
Sandstone	Eocene inf.	25	600	14	0.0710 (37)	0.8582 (447)	0.0278 (2068)	14±3	11		
Sandstone	Oligocene inf.	26	400	14	1.2991 (417)	1.2710 (408)	0.0278 (2068)	103±24	73		
Sandstone	Oligocene	28	400	22	0.2069 (113)	0.2228 (110)	0.0261 (1944)	155±30	58		
Sandstone	Miocene inf.	30	380	64	0.2813 (745)	0.9826 (2602)	0.0278 (2068)	47±4	44		
Sandstone	Cret. sup.	31	700	29	0.0351 (53)	1.1012 (1661)	0.0278 (2068)	5±1	24	12.7±2.3	17
Schistone	-	32	700	22	0.2893 (175)	0.3257 (197)	0.0255 (2273)	134±18	31		
Sandstone	Oligocene	33	700	32	0.5923 (529)	0.9909 (885)	0.0255 (2273)	88±8	18		
Schistone	-	34	700	25	0.7503 (1067)	2.0208 (2874)	0 0255 (2273)	56±4	14	11.2±1.6	100
Sandstone	Vrac-Cenom.	45	800	81	0.3916 (1947)	0.8223 (4089)	0.0255 (2273)	72±5	17		
Sandstone	Miocene	47	700	100	0.6456 (2273)	1.1072 (3898)	0.0255 (2273)	85±6	31		
Sandstone	Eocene	48	1280	84	0.0692 (206)	0.9160 (2728)	0.0255 (2273)	12±1	14	8.1±2.8	4
Sandstone	Miocene inf.	50#	600	72	0.5254 (1250)	1.7111 (4071)	2.5342 (4611)	38±10	67		
Sandstone	Oligocene inf.	51#	590	45	0.1641 (358)	2.6352 (5749)	2.5342 (4611)	9±2	12	13.1±1.82	47
Schist	-	52#	2130	51	0.0124 (41)	0.1449 (478)	2.5342 (4611)	12±4	16		
Sandstone	Paleo-Eocene	56	450	18	0.9222 (640)	1.1153 (774)	0.0277 (1975)	126±18	49		
Sandstone	Oligocene	57	530	7	0 9291 (194)	1.1780 (246)	0.0277 (1975)	115±22	37		
Schist	-	58	770	45	0.0040 (10)	0.0535 (135)	0.0260 (2009)	11±4	14		
Schist	-	60	830	46	0.0068 (16)	0.0675 (159)	0.0260 (2009)	17±5	89		
Sandstone	Paleocene	64#	430	92	0.1993 (660)	1.0593 (3508)	2.5342 (4611)	27±7	43		
Sandstone	Eocene	65#	500	55	0.2684 (487)	1.6385 (2973)	2.5342 (4611)	21±6	84		
Sandstone	Oligocene	66#	620	100	0.1955 (938)	1.1586 (5558)	2.5342 (4611)	24±6	48		
Sandstone	Eocene	67#	630	115	0.1302 (533)	1.3900 (5689)	2.5342 (4611)	12±3	99		
Sandstone	Albian	68#	680	44	0.1191 (351)	1.0055 (2963)	2.5342 (4611)	16±4	49		
Sandstone	Paleogene inf.	69#	370	77	0.0950 (854)	0.8019 (4085)	2.5342 (4611)	30±8	52		
Sandstone	Miocene inf.	70#	250	53	0.5087 (2044)	1.4264 (5732)	2.5342 (4611)	52±13	34		
Sandstone	Cretaceous	72#	520	75	0.0768 (282)	0.9685 (3609)	2.5342 (4611)	11±3	16	12.7±1.5	47
Sandstone	Albian	73#	680	52	0.0630 (164)	0.9855 (2566)	2.5342 (4611)	9±2	11	12.8±2.1	45
Sandstone	Eocene	77#	600	73	0.0732 (291)	0.6646 (2643)	2.5342 (4611)	16±4	37		
Sandstone	Oligocene	78#	600	45	0.1080 (266)	1.8400 (4531)	2.5342 (4611)	8±2	15	13.7±1.0	19
Schist	-	80	835	44	0.3434 (896)	1.9314 (5040)	0.0260 (2009)	28±2	30	11.7±2.0	57
Schist	-	81	1240	27	0.2472 (511)	0.6985 (1444)	0.0260 (2009)	53±4	14	11.2±1.7	84
Schist	-	82	620	38	0.1484 (386)	0.3422 (890)	0.0260 (2009)	50±9	78		
Schist	-	85	620	41	0.0616 (167)	1.1130 (2868)	0.0260 (2009)	9±1	47		
Sandstone	Cret. inf.	86	640	9	0.7294 (439)	0.6347 (382)	0.0260 (2009)	76±31	100		
Tuff	Miocene M+inf.	88	380	36	0.1272 (343)	1 3840 (3731)	0.0260 (2009)	14±1	21	14.0±0.7	7
Tuff	Oligo-Miocene	89	600	8	0.1076 (67)	0.5926 (369)	0.0260 (2009)	27±5	31		
Sandstone	Paleogene	106	900	48	0.0604 (193)	0.8840 (3147)	0.0353 (2460)	13±1	26		
Sandstone	Paleogene	107	1030	86	0.1597 (938)	1.7888 (10507)	0.0353 (2460)	22±2	78		

Personal ζ used of C. Sanders is 11733 ± 589; ζ of P. Andriessen (samples labeled with an asterisk) is 11,134 ± 334, both with Fish Canyon standard apatite and dosimeterglass 963. For Fish Canyon apatite and dosimeter CN-2 (labeled with #) ζ=111±22 for C. Sanders. Irradiation took place at the low flux reactor (fluence 5x 10^{15}) at Energie Centrum Nederland in Petten (NL). N is the number of grains counted; Rho s, Rho i, and Rho d are spontaneous, induced, and dosimeter track densities (tracks x 10^6/cm^2) with number of tracks in brackets. Central age (C.A.) is in Ma, dispersion (Disp.) is in percentages, mean track length is in μm±1σ, and number of measured confined tracks N,L.

Miocene FT history of the various samples (volcanic tuff versus clastic sediments of various stratigraphic ages), or an anomalous but poorly constrained FT age (profile C-C').

7.2. Thermal History and Timing of Cooling Phase

Thermal histories can be evaluated by combining apparent apatite FT central ages and track length distributions measured (in μm) on horizontally confined tracks [*Gleadow et al.*, 1986; *Laslett et al.*, 1987; *Green et al.*, 1989; *Crowley et al.*, 1991]. We used the Monte Trax program with the Laslett Durango annealing model [*Laslett et al.*, 1987; *Laslett and Galbraith*, 1996] to constrain the thermal histories with the inverse genetic algorithm model [*Gallagher et al.*, 1991; *Gallagher*, 1995].

A disadvantage of most East Carpathian samples is the lack of large numbers of fossil track lengths needed for detailed thermal history analysis. Also, samples displaying a high amount of grain age dispersion cannot be thermally modeled because the inverse model demands that all apatite grains anneal similarly under uniform T conditions (chemistry) and experienced the same FT history (provenance).

The total-reset samples are used to reconstruct the post-burial cooling history. In the northern and central segments

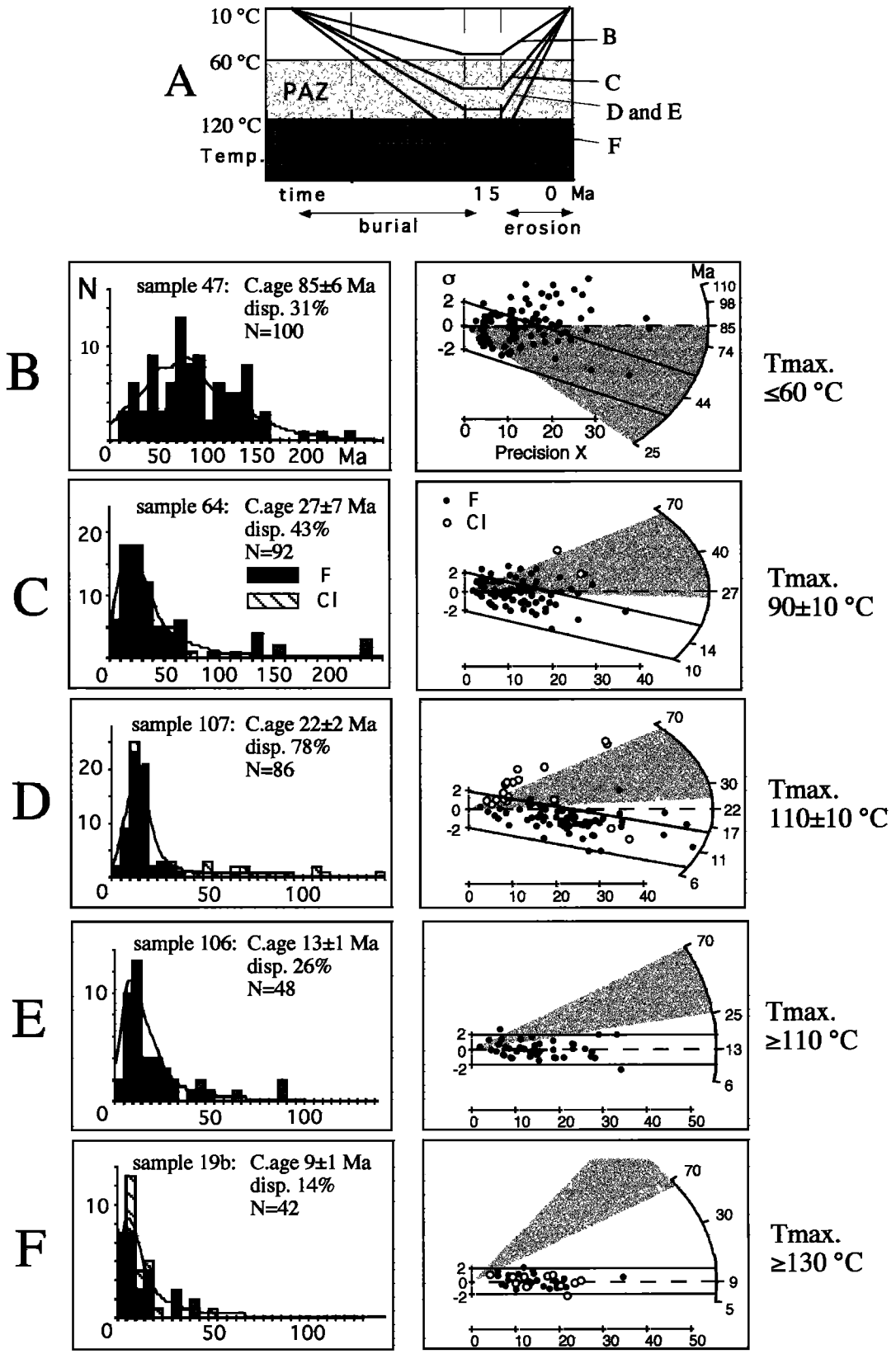

Figure 7. Figure 7a Thermal histories from the East Carpathians. Figures 7b-7f Five samples representing thermal histories from Figure 7a. The degree of annealing increases from top to bottom. Left column diagrams are single grain age distribution histograms. Gray shading marks F apatite; hatching marks F-Cl-OH apatite, based on etch pit dimensions. Right column diagrams are radial plots of the same samples. Gray shading marks stratigraphic age; solid circles mark F apatite; open circles mark F-Cl-OH apatite grain ages. The dashed line is FT central age. Open bar represents minimum age ±2σ.

Table 2. Etch conditions and Paleotemperature Estimates

Sample	t Etch, s	T Etch, °C	Etch Pits, μm	Chemistry	Max Paleo T, °C	Paleodepth, km
3	±25	20-25	no	?	60	2.5
4	±25	20-25	no	?	110±10	5±0.5
5	±25	20-25	no	?	90±10	4±0.5
6	±25	20-25	no	?	80±10	3.5±0.5
15	25	20-25	0.5-1 5	F	60	2.5
16	25	22	0.5-3.0	mix F-Cl	110±10	5±0.5
17	25	22	0.5-3.0	mix F-Cl	110±20	5±1
18I	25	22	no	?	110±20	5±1
18II	32	23	no	?	110±20	5±1
19	25	19	no	?	110±10	5±0.5
19b	25	22	0.5-3.5	mix F-Cl	130	6
21	25	21	no	?	110±20	5±1
23	25	22	0.5-3.5	mix F-Cl	100±10	5±0.5
24	25	22	0.5-2.5	mix F-Cl	120	5.5
25	25	22	0.5-2.5	mix F-Cl	120	5.5
26	25	20-25	no	?	60	2.5
28	25	22	no	?	60	2.5
30	25	20-25	0.5-1.5	F?	80	3.5
31	25	22	1.0-2.5	mix F-Cl	120	5.5
32	20	25	0.5	F	60	2.5
33	23	25	0.5-1.5	F	60	2.5
34	20	25	0.5-1.5	F	60	2.5
45	20	25	0.5-1.5	F	60	2.5
47	20	25	0.5-1.5	F	60	2.5
48	23	25	0.5-2.5	mix F-Cl	110±10	5±0.5
50	20	25	0.5-1.5	F	60	2.5
51	23	25	0.5-2.5	mix F-Cl	120	5.5
52	23	25	0.5-1.0	F	110±10	5±0.5
56	25	21	0.5-1.5	F	60	2.5
57	25	21	0.5-1.0	F	60	2.5
58	32	23	no	F?	110±10	5±0.5
60	32	23	no	F?	110±10	5±0.5
64	20	25	0.5-2.5	mix F-Cl	90±10	4±0.5
65	21	25	0.5-2.5	mix F-Cl	100±10	4.5±0.5
66	20	25	0.5-2.5	mix F-Cl	100±10	4.5±0.5
67	20	25	0.5-2.5	mix F-Cl	110±10	5±0.5
68	23	25	0.5-1.5	F	100±10	4.5±0.5
69	20	25	0.5-1.5	F	100±10	4.5±0.5
70	20	25	0.5-2.5	mix F-Cl	60	2.5
72	23	25	0.5-1.5	F	110	5
73	23	25	0.5-1.0	F	110	5
77	20	25	0.5	F	100±10	5±0.5
78	22	25	0.5-2.0	mix F-Cl	120	5.5
80	32	23	0.5-1.5	F	90±10	4±0.5
81	30	23	1.0-1.5	F	90±10	4±0.5
82	32	23	1	F	80±20	3.5±1
85	30	23	1	F	110	5
86	32	23	0.5-1.5	F	80±20	3.5±1
88	25	23	0.5-2.0	mix F-Cl	70±10	3±0.5
89	30	23	0.5-2.5	mix F-Cl	80	3.5
106	32	22	0.5-1.5	F	110	5
107	32	22	0.5-2.5	mix F-Cl	110±10	5±0.5

Apatite mounts were etched with 5N HNO_3 (etch time in seconds) to make tracks microscopically visible (Etchant Temperature in °C). A mean value of the long axes of etch pits was estimated for each grain (in bins of 0.5 μm). Presented etch pit values are variations among grains in a sample. Chemistry is based on Etch pits. Etch pits ≤1.5 are grouped as F-rich apatites. Paleodepth is based on paleogeotherm of 20 °C/km and a surface temperature 10 °C.

(profile A-A' to C-C') of the mountain chain these samples have similar ages between 8 and 14 Ma. Six of these samples with sufficient track lengths gave mean lengths from 12.7±1.5 to 13.5±2.3 μm (Table 1) and wide track length distributions (inset Figure 8) yielding roughly identical thermal histories (Figures 8a-8d). The onset of cooling from 120°-130°C started during late Badenian to Sarmatian (15-11 Ma) with more or less constant cooling rates until the present day. Modeling with the Crowley F apatite model yielded somewhat younger onsets of cooling and faster cooling rates (illustrated in Figure 8e), but also higher paleotemperatures, which is in contradiction to the observation that F apatites anneal more readily. Therefore preference is given to the well-established Laslett Durango model [*Laslett and Galbraith*, 1996] for our interpretation. Besides a Miocene phase, a well-constrained Late Cretaceous cooling phase is recorded in the thermal history of the crystalline schist of the Outer Dacides (Figure 8 f).

7.3. Minimum Ages (Multicomponent Populations)

In the case of partially annealed samples with high grain age dispersion, inverse modeling could lead to misinterpretation of thermal histories. We use instead the grain age distribution within these samples to obtain the onset of the cooling event. For samples residing at temperatures between 100° and 120°C (which is the case for many samples of the East Carpathians; see below), the track record of the F apatites was totally erased, while Cl apatites still preserved a significant part of the record of an older history [*Green et al.*, 1986; *O'Sullivan and Parrish*, 1995]. Upon cooling the once totally annealed F apatites start to retain tracks again, and their FT age represents a minimum estimate for the onset of cooling.

The grain age population of a sample with high dispersion can be described by a number of statistically distinct components (usually two or three) [*Galbraith and Green*, 1990]. Because the differential annealing behavior of apatites is not only dependent on the Cl-F ratio [e.g., *Ravenhurst et al.*, 1992] and not completely understood, it is useful to decompose high-dispersion populations irrespective of a demonstrable relation with the Cl-F content.

We calculated the number of components and the age of each component using the Fat Mix program based on *Sambridge and Compston* [1994] (see Figure 9). It is preferred to have analyzed 40-100 apatite grains to get statistical meaningful results and to prevent incidental features based on a few grains. Samples yielding significantly different components are presented in Table 3. The youngest component is called the minimum age [see also *Galbraith and Laslett*, 1993] and the older components are ignored for interpretation.

In the northern and central part of the orogen the minimum ages correspond well to the lowest FT central ages (as would be expected since both are presumably reset ages) clustering around 11 (±3) Ma (Figure 2). In the Bend Zone, however (profile D), the well-defined minimum ages decrease gradually from the toe of the prowedge toward the outer-arc-high, where they are as young as 2 Ma (see Figure 10). Although these minimum ages are not track length corrected they indicate an approximate Pliocene cooling age. This is confirmed by track length modeling of the totally reset sample 31 (Figure 10), which yields a near-linear Pliocene cooling phase.

7.4. Maximum Temperature

One of our goals is to determine the amount of erosion across the orogen in order to study the relationship between the erosion pattern and the wedge geometry. This involves two assumptions. First, cooling of rocks took place entirely by erosion. This is a reasonable assumption since no evidence for tectonic unroofing [cf. *Platt*, 1986] is found in the East Carpathians. Second, we assume that the geothermal gradient was constant and uniform in time and space. We discuss this assumption in more detail later. We determine the amount of section removed by estimating paleotemperatures from the FT data. In the case where track length measurements are not

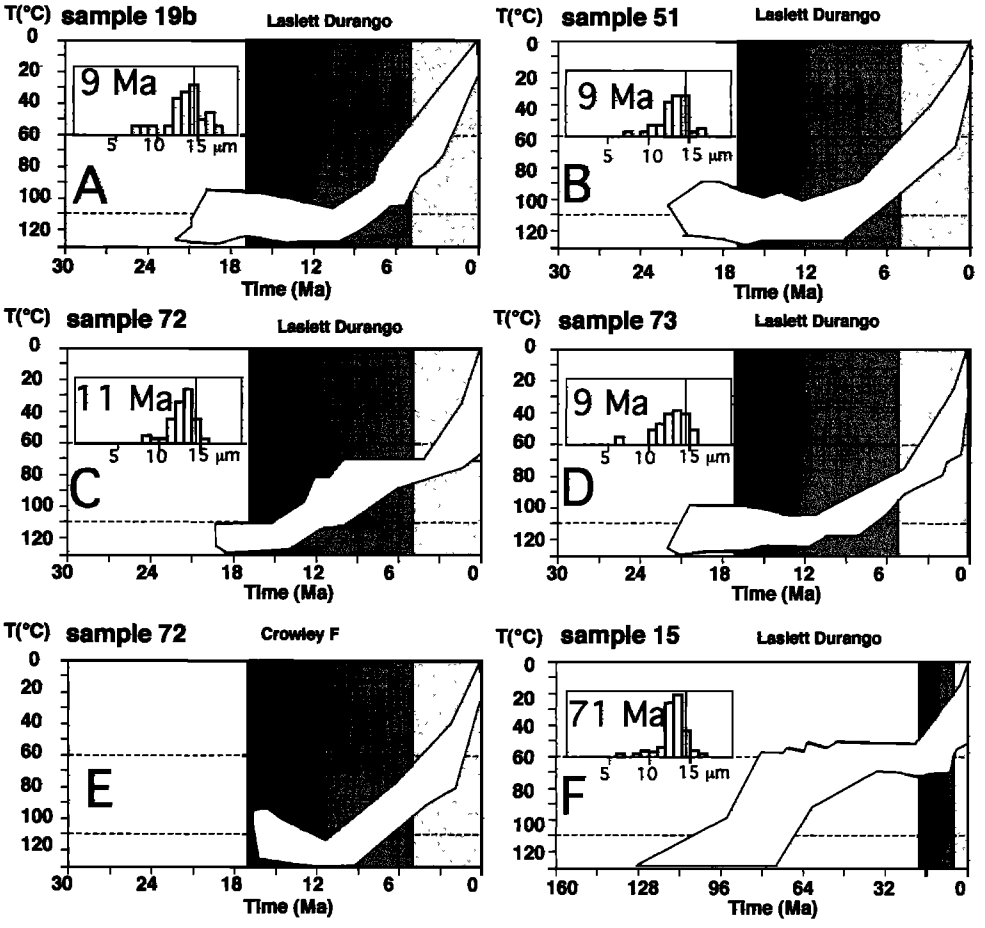

Figure 8. Thermal histories of selected samples. Dark gray is Badenian (17-12 Ma); gray is Sarmatian to Pannonian (12-5 Ma); and light gray is Pliocene-Quaternary (5-0 Ma). Figures 8a-8d are sediments with thermal histories based on the Durango annealing model; Figure 8e is same sample as Figure 8c but with Crowley annealing model; Figure 8f is thermal history of crystalline basement in the East Carpathians. Length distribution histograms and FT central age are plotted in the left upper corner (vertical reference line is the thermally unaffected length of 14.5 μm)

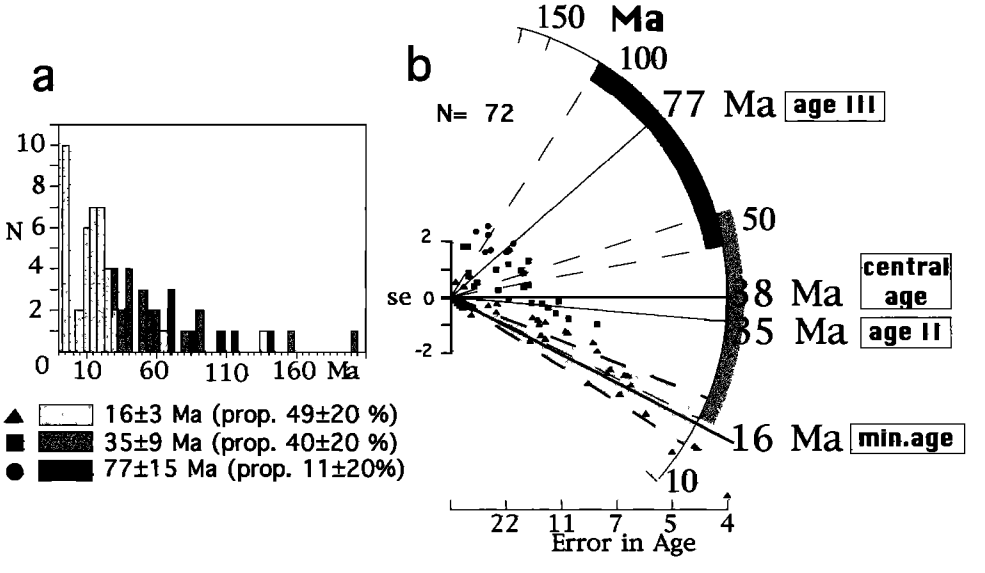

Figure 9. Example (sample 50) of grain age distribution histogram (Figure 9a) subdivided in three components. Component ages and relative proportions are noted below the plot. Figure 9b shows the radial plot of the same sample. The age is in Ma on radial axes. Individual grain ages can be read by a line from origin, through black notation to the radial axes. Horizontal axes are error in age in Ma for each grain. Vertical axes are standard deviation (σ) applicable to each grain.

Table 3. Significant Results of Calculations Carried Out With the Fat MIX Program

Sample	Min Age 1, Ma	Age 2, Ma	Age 3, Ma	% 1-2-3
16	14±2	(66±37)	_	97-03
23	14±5	25±8	_	56-44
45	50±4	73±3	_	31-69
47	44±4	84±4	132±13	31-57-12
50	16±3	29±6	67±10	44-36-20
64	14±2	26±3	_	52-48
65	6±2	15±2	_	27-73
66	4±1	20±1	_	11-89
67	2±1	6±1	23±5	17-18-65
68	7±3	13±7	19±5	39-35-26
69	11±1	30±5	41±17	43-46-11
69	8±2	17±2	42±8	12-62-26
70	33±4	47±4	_	30-70
77	11±1	(17±58)	_	99-01
107	11±2	17±3	(77±7)	62-31-07

Only samples with dispersion >30% and containing more than 40 grains were decomposed using the Laslett model with Gaussian errors Generally, 15 runs of 15 iterations were performed to maximise the number of components and to check the reproducibility. In a good sample, runs produce similar components within the error margins (except sample 69) Components with abundances <10% (e.g., 77 and 16 in parentheses) were neglected (because of the effects of a few extreme grain ages).

available we use the relation between FT ages and the stratigraphic ages of the sediments. For the sediments in the flysch basins, burial (and therefore heating) took place by continued sedimentation and, subsequently, by nappe stacking in the deforming wedge (Figure 7a). As long as sediments remain at low T (<60°C), they contain FT grain ages older than, or at best equal to, their stratigraphic ages (FT "source ages" or "provenance ages"; see Figure 7b). With increasing temperatures in the PAZ the fission tracks are increasingly annealed, the F-rich apatites more readily than the Cl apatites. The FT ages correspondingly decrease and eventually become younger then the stratigraphic age ("intermediate ages"; see Figures 7c-7d). Above 110°C no tracks are retained in F apatites and the FT age is completely reset (see Figure 7e). The Cl apatites are reset at 130°C (see Figure 7f). Once the onset of postburial cooling is known to be at ±12 Ma (Figures 7e-7f), we can run a forward model with the Monte Trax program and simulate the relationship between FT ages and the stratigraphic ages. This yields estimates of the maximum temperature a sample has experienced during the Miocene with errors at best of ±10°C. The results are presented in Table 2. We used stratigraphic ages published on geological maps, recalibrated by *Rögl* [1996] for the Central Para-Tethys. The metamorphic rocks of basement schist have no such reference point as a stratigraphic age, but they ultimately always come from deeper in the crust (TAZ). The maximum temperature during the Miocene is evaluated from track length modeling or the timing of the previous resetting event, which is Cretaceous (Figure 8f). The maximum temperature estimates are converted to a paleodepth by

$$z_p=(T_{max}-T_s)/T'_0$$

where z_p is paleodepth, T_{max} is the maximum paleotemperature, T_s is the surface temperature and T'_0 is the applied geotherm. Here we applied a paleogeotherm T'_0 of 20°C/km (for the former flysch basin and the subsequent thrust belt) and a surface temperature T_s of 10°C. These estimates are reasonable since geotherms of old passive margins are generally cool [cf. *Desegaulx et al.*, 1991]. Today a fairly uniform heat flow (q_0) of 30-60 mW/m^2 exists over the entire East Carpathians [*Dövenyi and Horvath*, 1988; *Cranganu and Deming*, 1996; *Veliciu*, 1987], with the exception of the volcanic chain. Assuming a general thermal conductivity ($\kappa\rho c_v$) for schist, sand and argillite of 3.5 W/(m°C) [*Barr and Dahlen*, 1989] and using the relationship

$$q_0 = \kappa\rho c_v T'_0$$

this coincides with a present geotherm (T'_0) of 10°-20°C/km. Because of the uncertainties in the thermal conductivity (2-7 W/(m°C) and the presence of a few isolated measured geotherms around 20°C/km [*Dövenyi and Horvath*, 1988; *Veliciu*, 1987], we use a uniform paleogeotherm of 20(±5)°C/km to yield estimates of erosion.

The results are shown in Figure 5 where the erosion envelope is reconstructed by adding the paleo-overburden (z_p) to the sample elevation (Tables 1 and 2) and interpolating a curve between the results. Figure 5 shows that the erosion envelope (as well as the topography in Figure 4) is roughly a depressed mirrored image of the subsurface deforming wedge. Most material is eroded around the outer-arc-high (5-6 km) above the deepest part of the wedge. Erosion diminishes gradually to the peripheral foreland but rapidly (stepwise) to the retroforeland, which is best illustrated in sections D-D' and C-C'. The prowedge of profile A-A' shows a stepwise erosion curve coinciding with an abrupt ramp in the decollement with a vertical displacement of 2 km [see also *Mocanu et al.*, 1996]. Profile B-B' shows the same erosion pattern, but the ramp in the decollement fades laterally to the south and is less abrupt in profile B-B'.

During the period in which the East Carpathians were eroding, the peripheral foreland basin and the Transylvanian Basin were subsiding and receiving clastics (see below). Postdepositional erosion in these areas is on average less than 1 km, on the basis of sonic analysis and AFTT data from boreholes (G. De Broucker, personal communication, 1996; R. A. Donelick, personal communication, 1997) but possibly more at the basin margins where Miocene-Pliocene sediments are tilted and truncated [*Stefanescu*, 1985]. This information is incorporated in the erosion curves of Figure 5.

7.5. From Cooling Data to the Onset of Erosion

Erosion rates are relatively low in the East Carpathians (see below), and the samples were never buried deep below the critical isotherm of 120°C. As a result the onset of cooling can be directly converted to the onset of erosion [cf. *Brown and Summerfield*, 1997]. The main erosion phase in the northern and central segments started during the late Badenian-Sarmatian (15-11 Ma) and it continued approximately with the same rate until 5-0 Ma (Figures 8a-8d). Time-integrated erosion rates until the present are of the order of 0.5±0.1 mm/yr.

For the Bend Zone the main erosion phase started in the late Miocene-Pliocene (7-2 Ma; Figure 10). Time-integrated Pliocene-recent erosion rates for the Bend Zone are of the order of 1 mm/yr. *Barr and Dahlen* [1989] have shown that for the relatively low erosion and plate convergence rates we observed in the East Carpathian wedge a uniform undisturbed geotherm is a valid assumption.

7.6. Relation Between Erosion, Precipitation, and Topography

Erosion in an active critical Coulomb wedge essentially takes place as exhumation. *Barr and Dahlen* [1989] have

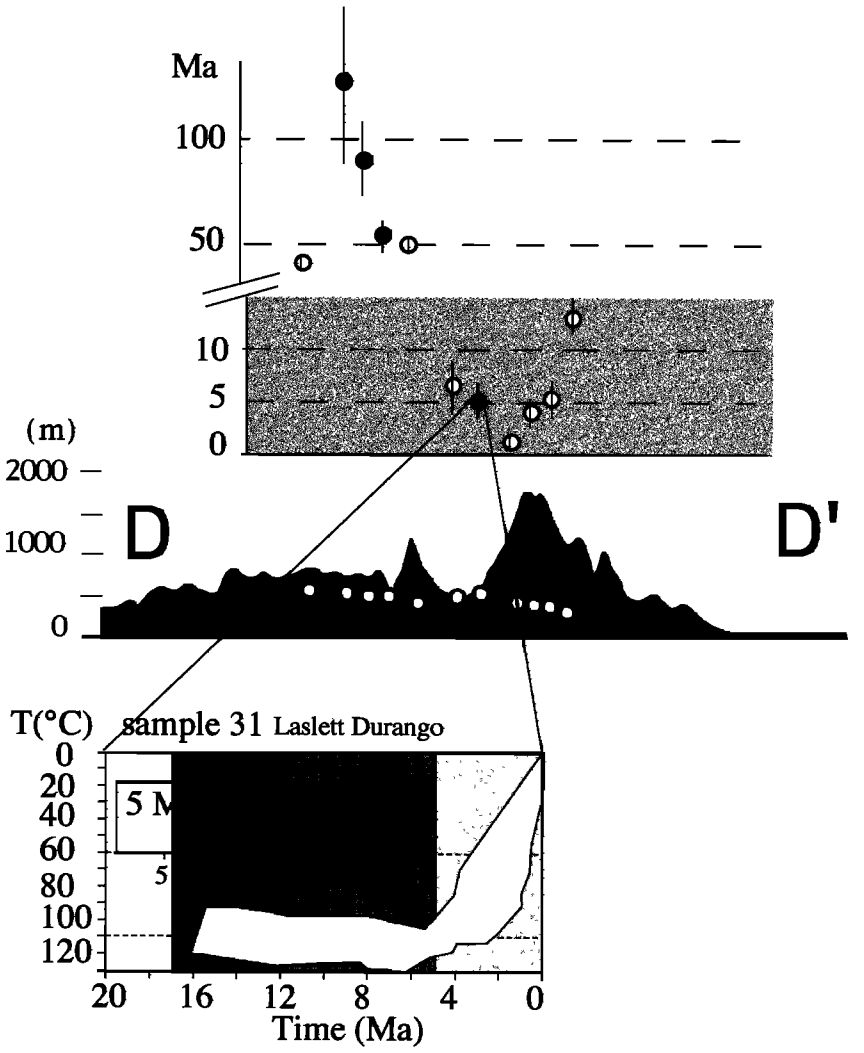

Figure 10. Profile D with calculated minimum FT ages (open circles) and totally reset central ages (solid circles). Note the break in age along the time axes. The inset thermal history of sample 31 is based on Laslett Durango annealing model.

shown that exhumation patterns of rocks in such wedges are principally determined by the erosion rate at the surface. The erosion rate, in turn, is dominated by local relief and precipitation. Local relief is highest in the core of the East Carpathians (vertical elevation of peaks to major river valleys reach up to 1000 m but averages at 500 m) and decreases gradually to the forelands, which is a common feature of orogens [e.g., *Ahnert*, 1984].

At present (and, we assume, during its Neogene history) both leeward and windward sides of the orogen receive similar amounts of precipitation of 800-1200 mm/yr, with the higher values restricted to the outer-arc-high [*Steinhauser*, 1970]. This precipitation pattern, combined with the local relief, predicts that the highest exhumation rates will occur symmetrically around the outer-arc-high. The FT data indeed show that the highest amounts of erosion took place in this part of the orogen.

8. Alternative Models

The combined approach of geometric and erosional constraints confirm the doubly vergent critical wedge concept as an appropriate orogen-forming mechanism for the East Carpathian fold-and-thrust belt. The erosion pattern coincides well with the independently constrained outline of the deforming wedge on the basis of topography and structures (Figure 5). The erosion pattern is consistent with the doubly vergent critical wedge models incorporating precipitation on both flanks of the orogen. Immediately neighboring areas are not involved in compressive deformation and thus not uplifted and eroded (Figure 1b). On the contrary, they subside and are areas of sediment deposition. Thus erosion patterns become a useful criterion for identifying deforming wedges, especially at places where other (geometric) methods are inconclusive. An actively deforming retrowedge for example, could not have been identified in the East Carpathians without the fission track results. The erosion pattern and timing of erosion as assessed with fission track analysis form a potential tool to distinguish between different geophysical models applied to natural settings.

Features like the formation of the outer-arc-high above the plate boundary, the erosion patterns related to the wedge geometry, the synorogenic erosion and sedimentation history, the (possible) flip of thrust vergence from the prowedge to the

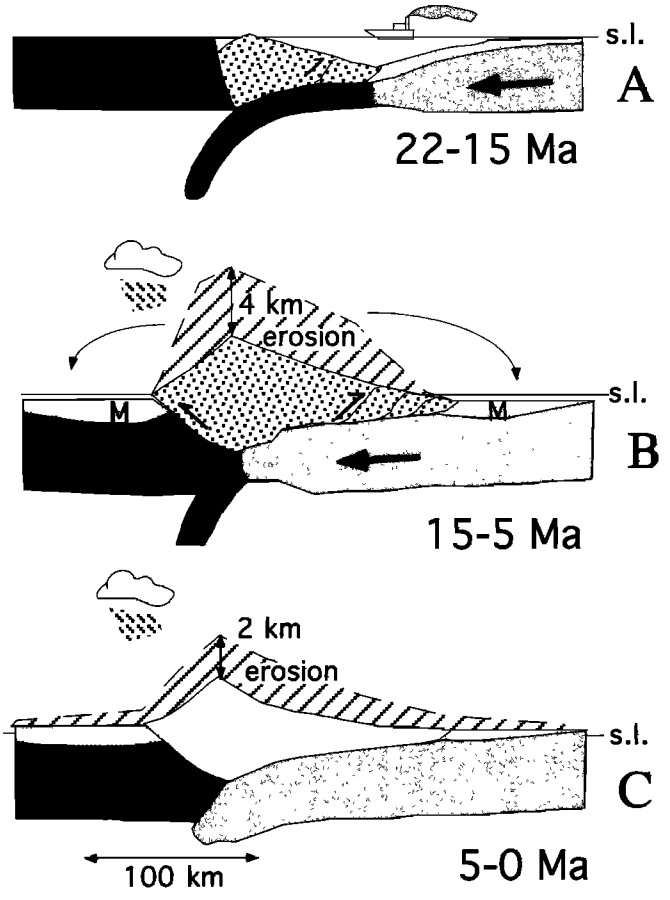

Figure 11. Three-phase wedge evolution (see text for explanation): (a) constructive wedge below sea level, (b) actively deforming wedge under influence of erosion; subsiding foreland basins, (c) destructive inactive wedge; general isostatic uplift of the region (note sea level marker). Dark and light gray areas are allochthonous and European lithosphere plates, respectively; black areas are oceanic lithosphere. Close stippled areas are actively deforming wedge; stippled areas (M) are foreland molasse basins.

retrowedge, and the relatively undeformed foreland and retroforeland are all consistent with the proposed concept. While individual features can be explained by other tectonic processes, no other tectonic models are known that can account for all of these features. Alternative models suggested by *Artyushkov et al.* [1996], the episodic accretion model from *Sandulescu* [1988], or the back-arc extension model from *Doglioni* [1992] are all inconsistent with the observed features and/or the erosion pattern.

9. A Three-Phase Wedge Evolution

Integrating the information on active structures, the erosion history from AFTT, and predictions based on the critical wedge concept, we can interpret the evolution of the East Carpathians in three distinct phases, where we focus on the northern and central parts of the East Carpathians and ignore the Bend Zone unless specifically stated. Thrusting in the East Carpathians (ss) has been active since the early Miocene [*Sandulescu,* 1988], which marks the onset of Neogene plate convergence. No erosion is recorded until the late Badenian, and the wedge probably grows in a self-similar way. The most likely reason for the absence of erosion is that the wedge remains below sea level. The underlying lithosphere is thought to be of oceanic origin with a substantial bathymetry [e.g. *Ellouz et al.,* 1994]. During the early active phase (20-15 Ma) the East Carpathians probably form an oceanic accretionary wedge which is in a constructive state (Figure 11a).

Acceleration of erosion rates took place during the late Badenian to Sarmatian (15-11 Ma). The sudden onset of high erosion rates is attributed to a change in the general subduction configuration (Figure 11b). The orogenic wedge is thrust over the threshold onto the European continental foreland plate [cf. *Jamieson and Beaumont,* 1988, *Stockmal et al.,* 1986], causing the wedge to rise high above sea level (needed to increase the erosion rate [*Ahnert,* 1984]). The onset of erosion evolves parallel to the diachronous evolution of the orogen from north to south, and always coincides with the final stage of deformation at its toe. It is documented that the last (Sarmatian) deformation phase in the East Carpathians (s.s.) is the most intensive of the three Miocene phases [*Sandulescu,* 1988; *Roure et al.,* 1993] and responsible for the main nappe emplacements and reactivation of out-of-sequence thrusts in the more internal regions of the orogen, pointing to a major rearrangement of the wedge in order to adapt to the change in the geometry of the frontal decollement. Because of the counterbalancing effect of erosion, the wedge tends to achieve a steady state width [e.g., *Dahlen and Barr,* 1989] during the Sarmatian to Pannonian (13-5 Ma).

The third phase is characterized by destruction. As soon as plate convergence ceases during the late Pannonian, no more material is stacked at the toe of the wedge, and the mechanism to maintain the critical taper no longer functions. Erosion, however, continues at approximately the same rate, and the wedge enters a state of destruction. The wedge becomes a passive landform which is gradually worn down by erosion processes. The destruction of the East Carpathians (ss) continued until the present day.

The gradual transition from a constructive to a steady state and finally to a destructive wedge is difficult to constrain with structures alone but is confirmed by the evolution of the foreland basins. A causal relation between foreland basins and wedge evolution is inferred on the basis of the axiom that orogens rest on a viscoelastic lithosphere plate which, in turn, floats on viscous asthenosphere [e.g., *Beaumont,* 1981]. The growing weight of the orogen downflexes the underlying lithosphere, creating a foredeep. Because of the doubly vergent character of the East Carpathians, foreland basins develop on either side of the orogen [e.g., *Johnson and Beaumont,* 1995]. The proforeland basin and the retroforeland basin (Transylvanian Basin) rapidly subside and receive large amounts of molasse sediments starting in the late Badenian-Sarmatian [*Meulenkamp et al.,* 1996; *Cranganu and Deming,* 1996]. The foreland basins thus record the growth and onset of rapid erosion of the East Carpathian orogen. As long as the orogen grows, the foreland basins continue to subside [*Jamieson and Beaumont,* 1988, *Peper et al.,* 1995]. No mass is lost in the region because of erosion of the orogen because mass is redistributed only over short distances (Figure 11b). The situation changes during the late Pannonian and the Pliocene. Docking has slackened the convergence between the two continental plates, causing the influx of material at the toe of the wedge to decrease. Erosion continues at approximately the same pace, and the orogen reduces in size while the foreland basins are filled with sediments to sea level. Subsequently, erosion products can no longer be stored in the

foreland basins and are transported over larger distances out of the region. The net mass loss in the region causes isostatic rebound [e.g., *Burbank*, 1992]. Sedimentation rates in the East Carpathian foreland basins are observed to decrease during the Pannonian [*Cranganu and Deming*, 1996], and since the Pontian (7-5 Ma) no sediments have been deposited. During the Pliocene and Quaternary the foreland basins are uplifted to a mean elevation of up to 400 m above sea level (Figure 11c). The evolution of the foreland basins thus suggests that the East Carpathian orogen was in a destructive state from Pliocene to present. A three-dimensional (3-D) isostatic and flexural numerical simulation based on the above described scenario confirmed the observed magnitude of the vertical motions in the retro-foreland basin [*Sanders*, 1998].

The amount of erosion associated with the Pliocene destruction can be approximated. River terraces in the East Carpathians range up to 1000 m above the present river beds. Estimated incision rates (taken as erosion rates) are of the order of 0.3±0.2 mm/yr [*Radulescu et al.*, 1996; *Artyushkov et al.*, 1996], somewhat less then long-term erosion rates deduced from fission track analyses (0.5-1 mm/yr). Extrapolating these rates to the entire Pliocene period yields a total amount of 1.5±1 km of erosion. If constant erosion rates are assumed on the basis of the AFTT data, approximately 2.5 km of erosion must have taken place over this period. Approximately 4±1 km of material is then left to account for exhumation during the active phases of the wedge (Figures 11b-11c).

In the Bend Zone, the erosion takes place simultaneously with active deformation in the wedge and subsidence of the proforeland basin (Focsani trough). The doubly vergent wedge in the Bend Zone is interpreted to be in a constructive or steady state throughout the Pliocene and Quaternary.

10. North-South Trend

The combined use of FT reset ages and reset FT minimum ages suggests that the East Carpathians and the Maramures area in the north have a uniform cooling record that starts in the late Badenian-Sarmatian (15-11 Ma). The Bend Zone in the south, however, is significantly younger, and erosion starts during the latest Pannonian-Pliocene (7-2 Ma). Our FT results thus support the general idea of a diachronous evolution of the East Carpathians from north to south.

The most northern wedge is not only older but also wider and shows different characteristics compared to the Bend Zone. The doubly wedge in profile A-A' consists largely of material from the allochtonous overriding plate (see Figure 5). Unlike current opinions wherein each deformation event is classified to a single tectogenetic unit, it is clear that the Outer Dacides, the Middle Dacides, and the Moldavides are all intensively involved in the Miocene deforming and eroding wedge. Here, even the area west of the retrowedge is significantly eroded (although the samples do not give an unequivocal signal), possibly pointing to the formation of a minimal tapered retro-foreland wedge, as shown by *Willet et al.*, [1993] and *Wang and Davis* [1996] for well-evolved doubly vergent critical wedges. Also, the Miocene deposits of the Transylvanian Basin show retrovergent compressive faulting in this corner [*Huismans et al.*, 1997; D.Ciulavu et al., manuscript in preparation, 1998].

In the two central profiles (B-B' and C-C') the range of allochtonous material involved in the wedge decreases southward while at the same time the orogen reduces in width (Figure 4). This is probably due to more evolved continent-continent collision in the northern part. In the Bend Zone the wedge is entirely made up of Neogene flysch and molasse, with possible but insignificant deformation and erosion in the Middle and Outer Dacides, displaying a more juvenile orogen. It remains unclear whether the transition to the more juvenile and younger Bend Zone is continuous or abrupt (fault bounded).

11. Conclusions

The combined use of structural studies, topography, and erosion patterns as reconstructed with AFTT suggests that the deformation history of the East Carpathians is dominated by a compressive orogenic frictional mechanism operative in the upper 10 km of the crust above a major decollement fault. Deformation is restricted to a doubly vergent wedge whose geometry is bounded by critical tapers. Incidental nappe emplacements previously referred to as separate "tectonic phases" are more likely caused by continuously converging plates during the Miocene.

During the early phase of Miocene convergence and thrusting, no significant erosion took place, and the wedge was below or close to sea level. Erosion rates accelerated in a late phase of plate convergence (15-11 Ma) and mark the climax of the deformation history. The major reorganization of the wedge is attributed to the arrival of the continental margin at the subduction zone. The erosion history was dominated by the interaction between the deformation mechanism and the external climatic conditions. As a result, substantial exhumation (up to 4 km) took place only over the actively deforming orogen. Neighboring areas were subsiding synchronously and received the clastics shed from the orogen.

During the Pliocene the wedge is in a destructive state because plate convergence ceased. Up to 2 km of erosion took place, leading to isostatic uplift of the region. The critical wedge geometry formed during the Miocene has been well preserved until the present day and only slightly reshaped by Pliocene-Quaternary erosion.

The Bend Zone in the south is characterized by an actively deforming wedge throughout the Pliocene. The erosion period lasts only 5±2 Ma when up to 5 km of material has been removed.

Compared to other well-studied examples of critical wedges like Taiwan and New Zeeland, the East Carpathians form a very modest orogen with moderate subduction, accretion, and precipitation rates, finally resulting in moderate exhumation rates. therefore thermal disturbances in the wedge are small [*Barr and Dahlen*, 1989], the elevation of the wedge is relatively low and structures like the major datachment zone along the retrowedge are not clearly developed or recognized.

Acknowledgments. C. Sanders is financially supported by the Netherlands Organisation for Scientific Research (NWO-GOA). P. Kamp, H. Kooi, R Huismans, and G. Bertotti are thanked for their fruitful discussion and comments on earlier drafts of the manuscript. F. Neubauer, M Roden-Tice, and M. Ellis are thanked for critical reviews that greatly helped to improve the manuscript. The University of Bucharest is thanked for support during field trips in Romania.

References

Ahnert, F., Local relief and the height limits of mountain ranges, *Am. J. Sci., 284*, 1035-1055, 1984.

Andriessen, P A.M., Fission track analyses: Principles, methodology and implications for tectono-thermal histories of sedimentary basins, orogenic belts and continental margins, *Geol. Mijnb., 74*, 1-12, 1995.

Artyushkov, E.V., M.A. Baer, and N.A Mörner, The East Carpathians: Indications of phase transitions, lithospheric failure and decoupled evolution of thrust belt and its foreland, *Tectonophysics, 262,* 101-132, 1996.

Balintoni, I., I. Gheuca, L. Nedelcu, L. Szasz, E. Nitoj, and I. Seghedi, Geol. Map Saru Dornei, 1:50,000, 33b, Inst de Geol. si Geofiz., Bucharest, 1982.

Barr, T.D., and F A. Dahlen, Brittle frictional mountain building, 2, Thermal structure and heat budget, *J. Geophys. Res., 94,* 3923-3947, 1989

Beaumont, C , Foreland basins, *Geophys. J. R. Astron. Soc., 65,* 291-329, 1981.

Beaumont, C., P. Fullsack, and J. Hamilton, Erosional control of active compressional orogens, in *Thrust Tectonics*, edited by K.R. McClay, pp. 1-18, Chapman and Hall, New York, 1992.

Beaumont, C , P.J.J. Kamp, J. Hamilton, and P. Fullsack, The continental collision zone, South Island, New Zealand: Comparison of geodynamical models and observations, *J. Geophys. Res., 101,* 3333-3359, 1996.

Bercia, I., E. Bercia, M. Sandulescu, and L. Szasz, Geol Map Vatra-Dornei, 1:50,000, 21d, Inst. de Geol. si Geofiz., Bucharest, 1975.

Brown, R W., Backstacking apatite fission track "stratigraphy". A method for resolving the erosional and isostatic rebound components of tectonic uplift histories, *Geology, 19,* 74-77, 1991.

Brown, R.W., and, M.A. Summerfield, Some uncertainties in the derivation of rates of denudation from thermochronological data, *Earth Surf. Pro. Landforms, 22,* 239-248, 1997

Burbank, D.W., Causes of recent Himalayan uplift deduced from deposited patterns in the Ganges basin, *Nature, 357,* 680-683, 1992.

Burchfiel, B.C., Eastern European alpine system and the Carpathian orocline as an example of collision tectonics, *Tectonophysics, 63,* 31-61, 1980.

Burtner, R.L., A. Nigrini, and R.A. Donelick, Thermochronology of Lower Cretaceous source rocks in the Idaho-Wyoming thrust belt, *AAPG Bull., 78,* 1613-1636, 1994.

Byrne, D.E., W. Wang, and D.M. Davis, Mechanical role of backstops in the growth of forearcs, *Tectonics, 12,* 123-144, 1993.

Chapple, W M., Mechanics of thin-skinned fold-and-thrust belts, *Geol. Soc. Am. Bull., 89,* 1189-1198, 1978.

Ciupagea, D., M. Pauca, and T. Ichim, *The Geology of the Transylvanian Depression* (in Romanian), 370 pp , Ed. Acad Repub. Soc. Romania, Bucharest, 1970.

Cranganu, C., and D. Deming, Heat flow and hydrocarbon generation in the Transylvanian basin, Romania, *AAPG Bull., 10,* 1641-1653, 1996.

Crowley, K.D., M. Cameron, and R.L. Schaefer, Experimental studies of annealing of etched fission tracks in fluorapatite, *Geochim. Cosmochim. Acta, 55,* 1449-1465, 1991.

Csontos, L., Tertiary tectonic evolution of the Intra-Carpathian area: A review, *Acta Vulcanol., 7,* 1-13, 1995.

Dahlen, F.A., Critical taper model of fold-and-thrust belts and accretionary wedges, *Annu. Rev. Earth Planet. Sci., 18,* 55-99, 1990.

Dahlen, F.A., and T D. Barr, Brittle frictional mountain building, 1, Deformation and mechanical energy budget, *J. Geophys. Res., 94,* 3906-3922, 1989.

Dahlen, F.A., J. Suppe, and D. Davis, Mechanics of fold-and-thrust belts and accretionary wedges: Cohesive coulomb theory, *J. Geophys. Res., 89,* 10,087-10,101, 1984.

Davis, D., J. Suppe, and F.A. Dahlen, Mechanics of fold-and-trust belts and accretionary wedges, *J. Geophys. Res., 88,* 1153-1172, 1983.

DeCelles, P G., & K.A. Giles, Foreland basin systems, *Basin Res., 8,* 105-123, 1996.

Desegaulx, P., H. Kooi, and S. Cloetingh, Consequences of foreland basin development on thinned continental lithosphere: Application to the Aquitaine basin (SW France), *Earth Planet. Sci. Lett., 106,* 116-132, 1991.

Dodson, M.H., Closure temperature in cooling geochronological and petrological systems, *Contrib. Mineral. Petrol., 40,* 259-274,1973.

Doglioni, C., Main differences between thrust belts, *Terra Res., 4,* 152-164, 1992

Dövenyi, P., and F. Horvath, A review of temperature, thermal conductivity, and heat flow data for the Pannonian Basin, in *The Pannonian Basin, A Study in Basin Evolution,* edited by L H. Royden and F Horvath, pp. 195-234, Am Assoc. of Pet. Geol , Tulsa, Okla., 1988.

Dumitrescu, I., O. Mirauta, M Sandulescu, M. Stefanescu, and T. Bandrabur, Bacau, *Geol. Map, 21,* 1:200,000, Geol. Inst., Bucharest, 1970.

Ellouz, N., and E. Roca, Palinspastic reconstructions of the Carpathians and adjacant areas since the Cretaceous: A quantitative approach, in *Peri-Tethyan Platforms,* edited by F. Roure, pp. 51-78, Ed. Technip, Paris, 1994.

Ellouz, N., F. Roure, M. Sandulescu, and D. Badescu, Balanced cross sections in the Eastern Carpathians (Romania): A tool to quantify Neogene dynamics, in *Geodynamic Evolution of Sedimentary Basins*, edited by F. Roure, N. Ellouz, V. S. Shein and I. Skvortsov, pp. 305-325, Technip, Paris, 1994.

England, P., and P. Molnar, Surface uplift, uplift of rocks, and exhumation of rocks, *Geology, 18,* 1173-1177, 1990.

England, P., and S. W. Richardson, The influence of erosion upon the mineral facies of rocks from different metamorphic environment, *J. Geol. Soc. London,* 134, 201-213, 1977.

Galbraith, R.F., and P.F. Green, Estimating the component ages in a finite mixture, *Nucl. Tracks Rad. Meas., 17,* 197-206, 1990

Galbraith, R.F., and G M. Laslett, Statistical models for mixed fission track ages, *Nucl. Tracks Rad. Meas., 21,* 459-470, 1993.

Gallagher, K., Evolving temperature histories from apatite fission-track data, *Earth Planet. Sci. Lett., 136,* 421-435, 1995.

Gallagher, K., M. Sambridge, and G. Drijkoningen, Genetic algorithms: An evolution from Monte Carlo methods for strongly nonlinear geophysical optimization problems, *J. Geophys. Res., 96,* 2177-2180, 1991.

Gleadow, A.J.W , and P.G. Fitzgerald, Uplift history and structure of the Transantarctic Mountains: New evidence from fission track dating of basement apatite in the Dry Valleys area, southern Victoria Land, *Earth Planet. Sci. Lett., 82,* 1-14, 1987.

Gleadow, A.J.W., I R Duddy, P F Green, and J.F. Lovering, Confined fission track lenghts in apatite: A diagnostic tool for thermal history analyses, *Contrib. Mineral Petrol., 94,* 405-415, 1986.

Green, P.F . Comparison of zeta calibration baselines for fission-track dating of apatite, zircon and sphene, *Chem. Geol., 58,* 1-22, 1985.

Green, P.F., The relationship between track shortening and fission track age reduction in apatite: combined influences of inherent instability, annealing anisotropy, length bias and system calibration, *Earth Planet. Sci. Lett., 89,* 335-352, 1988.

Green, P.F., I.R. Duddy, A.J.W. Gleadow, P.R. Tingate, and G.M. Laslett, Thermal annealing of fission tracks in apatite, 1. A qualitative description, *Chem. Geol., 59,* 237-253, 1986.

Green, P.F., I.R. Duddy, A.J.W. Gleadow, and J.F. Lovering, Apatite fission-track analyses as a paleotemperature indicator for hydrocarbon exploration, in *Thermal History of Sedimentary Basins-: Methods and Case Histories,* edited by N.D. Naeser, and T.H. McCulloh, pp. 181-196, Springer-Verlag, New York, 1989.

Griffiths, G.A., Some suspended sediment yields from South Island catchments, New Zealand, *Wat. Resources Bull., 17,* 662-671, 1981.

Horvath, F., Towards a mechanical model for the formation of the Pannonian basin, *Geophysics, 226,* 333-357, 1993.

Huismans, R.S., G. Bertotti, D Ciulavu, C. Sanders, S. Cloetingh, and C Dinu, Structural evolution of the Transylvanian Basin (Romania) A sedimentary basin in the bend zone of the Carpathians, *Tectonophysics, 272,* 249-268, 1997.

Hurford, A.J., and P.F Green, A user's guide to fission track dating calibration, *Earth Planet. Sci. Lett., 59,* 343-354, 1982.

Hurford, A.J , and P.F. Green, The zeta age calibration of fission-track dating, *Isot. Geosci., 1,* 285-317, 1983

Hyppolyte, J. C., and M. Sandulescu, Paleostress Characterization of the "Wallachian" phase in its type area (southeastern Carpathians, Romania), *Tectonophysics,* 263, 235-248, 1996.

Jamieson, R.A., and C. Beaumont, Orogeny and metamorphism: A model for deformation and pressure-temperature-time paths with application to the central and southern Appalachians, *Tectonics, 7,* 417-445, 1988.

Johnson, D.D., and C. Beaumont, Preliminary results from a planform kinematic model of orogen evolution, surface processes and the development of clastic foreland basin stratigraphy, in *Stratigraphic Evolution of Foreland basins, Spec. Publ. Soc. Econ. Paleontol. Mineral., 52,* 3-24, 1995.

Kamp, P.J.J , and J.M. Tippett, Dynamics of Pacific plate crust in the South Island (New Zealand) zone of oblique continent-continent convergence, *J. Geophys. Res., 98,* 16,105-16,118, 1993.

Kamp, P.J.J., P.F. Green, and S.H. White, Fission track analysis reveals character of collisional tectonics in New Zealand, *Tectonics, 8,* 169-195, 1989.

Kooi, K., and C. Beaumont, Large-scale geomorphology: Classical concepts reconciled and integrated with contemporary ideas via a surface processes model, *J. Geophys. Res., 101,* 3361-3386, 1996

Koons, P.O., Some thermal and mechanical consequences of rapid uplift: An example from the southern Alps, New Zealand, *Earth Planet. Sci. Lett., 86,* 307-319, 1987.

Koons, P.O., The topographic evolution of collisional mountain belts: A numerical look at the southern Alps, New Zealand, *Am. J. Sci., 289,* 1041-1069, 1989.

Koons, P.O., Two-sided orogen: Collision and erosion from the sandbox to the southern Alps, New Zealand, *Geology, 18,* 679-682, 1990.

Koons, P.O., Three-dimensional critical wedges: Tectonics and topography in oblique collisional orogens, *J. Geophys. Res., 99,* 12,301-12,315, 1994.

Koons, P.O., Modelling the topgraphic evolution of collisional belts, *Ann. Rev. Earth Planet. Sci, 23,* 375-408, 1995.

Krautner, H.G., F. Krautner, M. Sandulescu, I. Bercia, E. Bercia, G. Alexandrescu, M. Stefanescu, and J. Ion, Pojorita, *Geol. Map 21b,* 1:50,000, Inst. de Geol. si Geofiz., Bucharest, 1975.

Krautner, H.G., F. Krautner, L. Szasz, G. Udubasa, and G. Istrate, Rodna Veche, *Geol. Map 20d,* 1:50,000, Inst. de Geol. si Geofiz., Bucharest, 1978.

Laslett, G.M., and R.F. Galbraith, Statistical modelling of thermal annealing of fission tracks in apatite, *Geochim. Cosmochim. Acta, 60,* 5117-5131, 1996.

Laslett, G.M., P.F. Green, I.R. Duddy, and A.J.W. Gleadow, Thermal annealing of fission tracks in apatite, 2, A quantitative analysis, *Chem.Geol., 65,* 1-13, 1987.

Malavieille, J., Modelisation experimentale des chevauchement imbriques: Application aux chaines de montagnes, *Bull. Soc. Geol. Fr., 26,* 129-138, 1984.

Meulenkamp, J. E., M. Kovac, and I. Cicha, On Late Oligocene to Pliocene depocentre migrations and the evolution of the Carpathian-Pannonian system, *Tectonophysics,* 266, 301-317, 1996.

Mocanu, V.I., C. Dinu, F. Radulescu, M. Diaconescu, C. Diaconescu, and A. Pompilian, Seismogeological features of the crust in Romania, in *Oil and Gas in Alpidic Thrustbelts and Basins of Central and Eastern Europe*, edited by G. Wessely and W. Liebl, pp. 289-299, Am. Assoc. Pet. Geol., Tulsa, Okla., 1996.

Morley, C.K., Models for relative motion of crustal blocks within the Carpathian region, based on restorations of the Outer Carpathian trust sheets, *Tectonics, 15,* 885-904, 1996.

Muresan, M., S. Peltz, I. Seghedi, A. Szakacs, T. Bandrabur, H.G. Krautner, M. Sandulescu, G. Muresan, M. Peltz, and F. Krautner, Voslabeni, *Geol. Map 62a,* 1:50,000, Inst. de Geol. si Geofiz, Bucharest, 1986.

O'Sullivan, P.B., and R. Parrish, The importance of apatite composition and single grain ages when interpreting fission track data from plutonic rocks: A case study from the Coast Ranges, British Columbia, *Earth Planet. Sci. Lett., 132,* 213-224, 1995.

Pécskay, Z., et al., Space and time distribution of neogene-Quaternary volcanism in the Carpatho-Pannonian region, *Acta Vulcanol., 7,* 15-28, 1995.

Peper, T., R van Balen, and S. Cloetingh, Implications of orogenic wedge growth, intraplate stress variations, and eustatic sea-level change for foreland basin stratigraphy inferences from numerical modeling, in *Stratigraphic Evolution of Foreland Basins,* edited by S.L. Dorobek and G.M. Ross, pp. 25-36, Soc. for Sed. Geol., Tulsa, Okla., 1995.

Platt, J P., Dynamics of orogenic wedges and the uplift of high-pressure metamorphic rocks, *Geol. Soc. Am. Bull., 97,* 1037-1053, 1986.

Radulescu, F., V. Mocanu, V. Nacu, and C. Diaconescu, Study of recent crustal movements in Romania: A review, *J. Geodyn., 22,* 33-50, 1996.

Ratschbacher, et al., Cretaceous to Miocene thrusting and wrenching along the central southern Carpathians due to a corner effect during collision and orocline formation, *Tectonics, 12(4),* 855-873, 1993

Ravenhurst, C.E., and R.A. Donelick, Fission track thermochronology, in *Short Course Handbook on Low Temperature Thermochronology,* edited by M. Zentilli and P.H. Reynolds, pp. 21-42 Mineral. Assoc. of Can , Wolfville, 1992.

Rögl, F., Stratigraphic correlation of the Parathetys Oligocene and Miocene, *Mitt. Ges. Geol. Bergbaustud. Österr., 41,* 65-73, 1996.

Rohrman, M , Thermal evolution of the Fennoscandian region from fission track hermochronology: An integrated approach, Ph.D. thesis, Vrije Univ., Amsterdam, 1995.

Roure, F., E. Roca, and W. Sassi, The Neogene evolution of the outer Carpathian flysch units (Poland, Ukraine and Romania): Kinematics of a foreland/fold-and-thrust belt system, *Sediment. Geol., 86,* 177-201, 1993.

Sambridge, M.S., and W. Compston, Mixture modelling of multi-component data sets with application to ion-probe zircon ages, *Earth Planet. Sci. Lett., 128,* 373-390, 1994.

Sanders, C.A.E.., Tectonics and Erosion: Competitive forces in a compressive orogen. A fission track study of the Romanian Carpathians, Published Ph.D thesis, 204 pp., Vrije Univ. Amsterdam, Sept. 1998.

Sandulescu, M., Cenozoic tectonic history of the Carpathians, *AAPG Mem., 45,* 17-25, 1988.

Sandulescu, M., M., Muresan, and D. Muresan, Geol. Map 47d Damuc, 1:50,000, Inst. de Geol. si Geofiz., Bucharest, 1975.

Sandulescu, M., et al., Geological map of Romania, 1:1,000,000, Inst. de Geol. si Geofiz., Bucharest, 1978.

Sandulescu, M., M. Stefanescu, A. Butac, I. Patrut, P. Zaharescu, Genetical and structural relations between flysch and molasse (The East Carpathians Model), 95 pp., Inst. of Geol. and Geophys., Bucharest, 1981a.

Sandulescu, M., Kräutner, H.G., I. Balintoni, D. Russo-Sandulescu, and M. Micu, The structure of the East Carpathians (Moldavia-Maramures area), 92 pp., Inst. of Geol. and Geophys., Bucharest, 1981b.

Silver, E.A., and D.L. Reed, Backthrusting in accretionary wedges, *J. Geophys. Res., 93,* 3116-3126, 1988

Stefanescu, M., Elaborarea Profilelor, Scara 1:200.000 pentru completarea imaginii geologice a Teritoriului R. S. Romania (A-9,-10,-11,-12,-14,-18,-20), Inst. de Geol. si Geofiz., Bucharest, 1985.

Steinhauser, F., *Climatic Atlas of Europe, I: Maps of Mean Temperature and Precipitation,* World Meteorol. Organ., Geneva, 1970.

Stockmal, G.S., C. Beaumont, and R. Boutilier, Geodynamic models of convergent margin tectonics: Transition from rifted margin to overthrust belt and consequences for foreland-basin development., *AAPG Bull., 70,* 181-190, 1986.

Stüwe, K., L. White, and R. Brown, The influence of eroding topography on steady-state isotherms: Application to fission track analyses, *Earth Planet. Sci. Lett., 124,* 63-74, 1994.

Tippett, J M., and P.J.J. Kamp, Fission track analyses of the late Cenozoic vertical kinematics of continental collision, South Island, New Zealand, *J. Geophys. Res., 98,* 16,119-16148, 1993.

Torrini, R., and R.C. Speed, Tectonic wedging in the forearc basin-accretionary prism transition, Lesser Antilles forearc, *J. Geophys. Res., 94,* 10,549-10,584, 1989.

Veliciu, S., Geothermics of the Carpathian area, *Anu. Inst. Geol Geofiz., 67,* 81-117, 1987.

Wagner, G. A. and P. Van Den Haute, *Fission Track Dating,* 285 pp. Kluwer, Dordrecht, 1992

Wang, W.H., and D.M. Davis, Sandbox model simulation of forearc evolution and noncritical wedges, *J. Geophys. Res., 101,* 11,329-11,339, 1996.

Willet, S., C Beaumont, and P. Fullsack, Mechanical model for the tectonics of doubly vergent compressional orogens, *Geology, 21,* 371-374, 1993.

P. Andriessen, and S Cloetingh, Institute for Earth Sciences, De Boelelaan 1085, 1081 HV Amsterdam, Netherlands. (e-mail: andp@geo.vu.nl; cloeting@geo vu.nl)

C. Sanders, Midland Valley Exploration Limited, 14 Park Circus, G3 6 AX Glasgow, Scotland, UK (e-mail: carlo@mve.com)

(Received August 4, 1997; revised July 21, 1998,
accepted September 23, 1998.)